ARTICLE

IL-23 secreted by myeloid cells drives castration-resistant prostate cancer

Arianna Calcinotto[1], Clarissa Spataro[1], Elena Zagato[1], Diletta Di Mitri[1], Veronica Gil[2], Mateus Crespo[2], Gaston De Bernardis[1], Marco Losa[1], Michela Mirenda[1], Emiliano Pasquini[1], Andrea Rinaldi[1], Semini Sumanasuriya[2], Maryou B. Lambros[2], Antje Neeb[2], Roberta Lucianò[3], Carlo A. Bravi[3], Daniel Nava-Rodrigues[2], David Dolling[2], Tommaso Prayer-Galetti[4], Ana Ferreira[2], Alberto Briganti[3], Antonio Esposito[5], Simon Barry[6], Wei Yuan[2], Adam Sharp[2], Johann de Bono[2] & Andrea Alimonti[1,7,8,9]*

Patients with prostate cancer frequently show resistance to androgen-deprivation therapy, a condition known as castration-resistant prostate cancer (CRPC). Acquiring a better understanding of the mechanisms that control the development of CRPC remains an unmet clinical need. The well-established dependency of cancer cells on the tumour microenvironment indicates that the microenvironment might control the emergence of CRPC. Here we identify IL-23 produced by myeloid-derived suppressor cells (MDSCs) as a driver of CRPC in mice and patients with CRPC. Mechanistically, IL-23 secreted by MDSCs can activate the androgen receptor pathway in prostate tumour cells, promoting cell survival and proliferation in androgen-deprived conditions. Intra-tumour MDSC infiltration and IL-23 concentration are increased in blood and tumour samples from patients with CRPC. Antibody-mediated inactivation of IL-23 restored sensitivity to androgen-deprivation therapy in mice. Taken together, these results reveal that MDSCs promote CRPC by acting in a non-cell autonomous manner. Treatments that block IL-23 can oppose MDSC-mediated resistance to castration in prostate cancer and synergize with standard therapies.

Prostate cancer is the most commonly diagnosed cancer in males in the world and the second leading cause of mortality in males that is attributable to cancer[1]. After it was shown that androgens and androgen receptor (AR) signalling promote prostate cancer progression, androgen-deprivation therapy (ADT) has become the main prostate cancer therapy for patients at different stages of disease[2]. However, a considerable fraction of patients receiving such treatments ultimately progress to a more aggressive disease, developing CRPC[2]. The prognosis for patients with CRPC remains poor and the treatment of these patients remains a major unmet medical need[2–8]. A better understanding of the mechanisms that drive CRPC could identify more effective therapies. Deregulated AR signalling, induced by genomic amplification of the *AR* locus, AR splice variants and activation of co-regulators of the AR, is considered the major determinant of CRPC[2]. Activation of several AR-alternative signalling pathways also promotes CRPC[9,10]. However, these mechanisms suggest that cell-autonomous alterations occur in prostate tumour cells and do not take into consideration that these cells are surrounded by a complex tumour microenvironment. The well-established dependency of cancer cells on the tumour microenvironment[11] suggests that the non-cancer-cell component of the tumour may control prostate cancer progression, although the contribution of the tumour microenvironment, and in particular of the tumour immune response to the emergence of CRPC, remains unknown[12,13]. We and others have previously reported that MDSCs are a prominent immune cell subset infiltrating the CRPC microenvironment[14–16]. MDSCs are a heterogeneous population of activated immune cells that are expanded in pathological conditions, including cancer, and that have potent immunosuppressing activity[17]. On the basis of their expression markers, MDSCs can be classified into monocytic MDSCs or polymorphonuclear (PMN)-MDSCs[18]. Higher numbers of circulating

and tumour-infiltrating MDSCs have been observed in a large fraction of patients who have different types of tumours including prostate cancer[17,19,20]. MDSCs can support tumorigenesis by either suppressing the antitumour immune response or by promoting angiogenesis and senescence evasion in a number of contexts including prostate cancer[15,16,21]. MDSCs have been also found to be increased in patients that do not respond to ADT[20]. However, whether MDSCs support androgen-independent tumour growth and the emergence of CRPC remains unknown. Here, we show that IL-23 secreted by increased numbers of MDSCs in both human and mouse prostate tumours can confer androgen independence in a non-cell autonomous manner through the activation of AR signalling. Inhibition of IL-23 or IL-23 receptor signalling in these tumours restores sensitivity to ADT.

MDSCs confer castration resistance

By analysing biopsies from patients with castration-sensitive prostate cancer (CSPC) and CRPC, we found that PMN-MDSCs (CD11b+CD33+CD15+ cells)[18] were enriched in CRPC and localized in close proximity to EpCAM+ epithelial tumour cells (Fig. 1a and Extended Data Fig. 1a). Notably, increased PMN-MDSCs in tumours were not associated with increased levels of CD11b+CD15– cells (Extended Data Fig. 1b). Therefore, we hypothesized that tumour infiltrating PMN-MDSCs could directly contribute to the emergence of CRPC. We investigated this hypothesis using the *Pten*-null prostate conditional knockout (*Pten^{PC−/−}*) mouse model and two additional allograft models of prostate cancer (TRAMP-C1 and MyC-CaP) that develop tumours driven by *Pten* loss, p53 and RB inactivation, and MYC amplification, respectively[2]. As previously reported[22], surgical castration of *Pten^{PC−/−}* mice leads to initial tumour regression (castration-sensitive phase, *t* = 4 weeks) followed by tumour progression and emergence

[1]Institute of Oncology Research (IOR), Oncology Institute of Southern Switzerland, Bellinzona, Switzerland. [2]The Institute of Cancer Research and The Royal Marsden NHS Foundation Trust, London, UK. [3]Division of Oncology, Unit of Urology, URI, IRCCS Ospedale San Raffaele, Milan, Italy. [4]Department of Urology, University of Padova, Padova, Italy. [5]Experimental Imaging Center, San Raffaele Scientific Institute, Milan, Italy. [6]IMED Oncology AstraZeneca, Li Ka Shing Centre, Cambridge, UK. [7]Università della Svizzera italiana, Faculty of Biomedical Sciences, Lugano, Switzerland. [8]Faculty of Biology and Medicine, University of Lausanne UNIL, Lausanne, Switzerland. [9]Department of Medicine, Venetian Institute of Molecular Medicine, University of Padova, Padova, Italy. *e-mail: andrea.alimonti@ior.iosi.ch
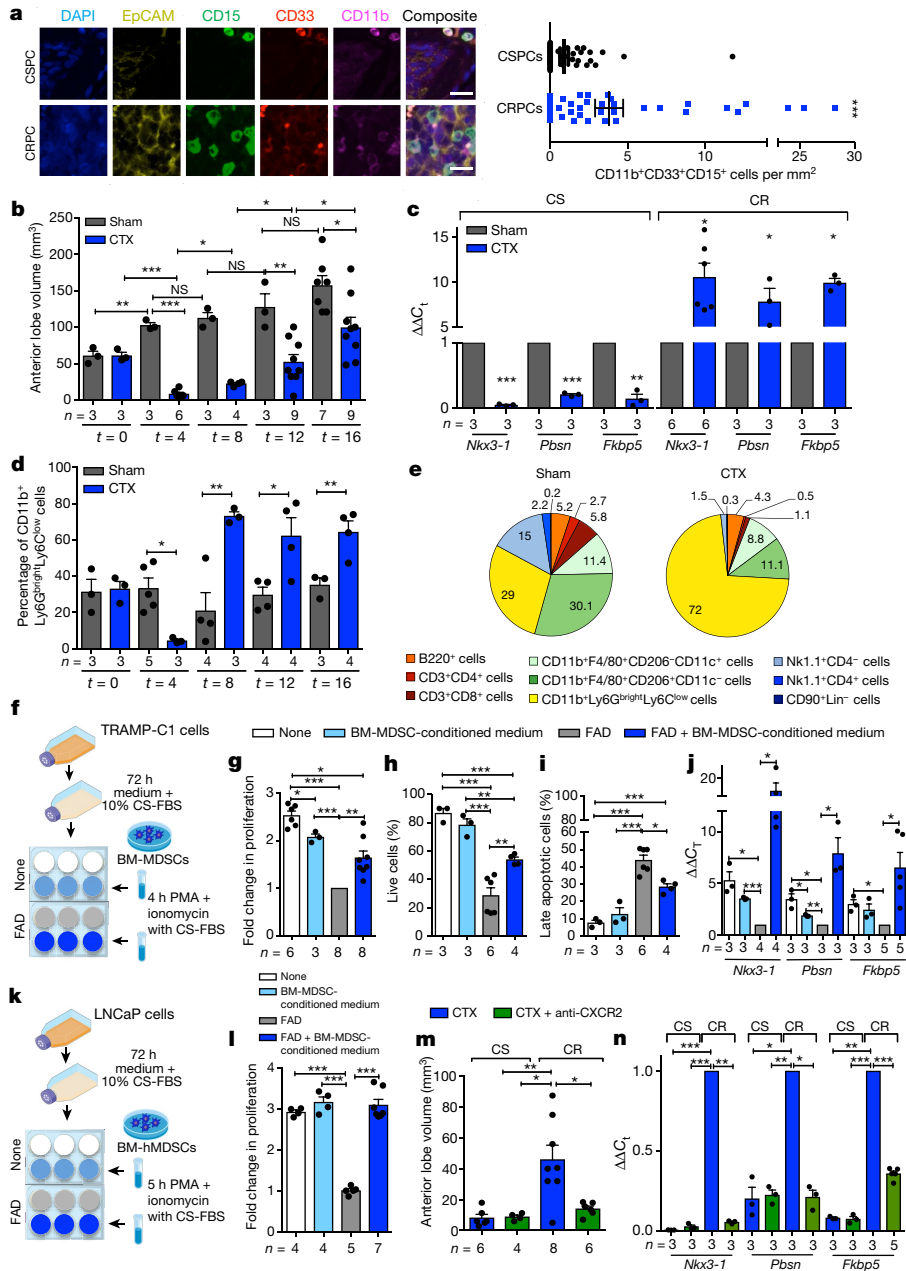
Fig. 1 | MDSCs infiltrate CRPC paralleling the activation of AR pathway and conferring resistance to castration to prostate cancer. **a**, CD11b^{+}CD33^{+}CD15^{+} PMN-MDSCs within the tumours of patients with CSPC or CRPC. Left, representative images of CSPC and CRPC from patient 1. Right, Quantification. EpCAM, yellow; CD15, green; CD33, red; CD11b, pink; DAPI, blue. $n = 51$ biologically independent patients per group reported; data are mean ± s.e.m. Statistical analyses (negative binomial regression model): $P < 0.001$. **b–d**, $Pten^{PC-/-}$ mice that were sham-operated (Sham) or surgically castrated (CTX) $Pten^{PC-/-}$ mice at different time points. **b**, Tumour volume of the anterior prostate lobe. **c**, Quantitative PCR with reverse transcription (qRT–PCR) analyses of the indicated genes in the prostate tumours at $t = 4$ weeks (castration-sensitive phase (CS)) and $t = 12$ weeks (castration-resistant phase (CR)). **d**, Flow cytometry for tumour PMN-MDSCs (gated on CD45^{+} cells). **e**, Percentages of tumour-infiltrating immune cell populations (gated on CD45^{+} cells). **f**, Experimental schematic. CS-FBS, charcoal-stripped

FBS. **g**, TRAMP-C1 cell proliferation. **h**, Percentage of annexin V^{−} and 7-aminoactinomycin D (7AAD)-negative TRAMP-C1 cells. **i**, Percentage of annexin V[+] and 7AAD[+] TRAMP-C1 cells. **j**, qRT–PCR analyses of the indicated genes in TRAMP-C1 cells. **k**, Experimental schematic. PMA, phorbol myristate acetate. **l**, Proliferation of LNCaP cells. **m**, Volume of prostate tumours of CTX $Pten^{PC-/-}$ mice treated with the CXCR2 antagonist or untreated at the end of the study (12 weeks after CTX). **n**, qRT–PCR analyses of the indicated genes in the prostate tumours of mice treated as in **m**. Specific n values of biologically independent mice (**b–d**, **m**, **n**) and independent samples (**g–j**, **l**) are shown and data are mean ± s.e.m. **b**, **d**, **h**, **i**, **l**, **m**, Statistical analyses (unpaired two-sided Student's t-test): NS, not significant; $*P < 0.05$; $**P < 0.01$; $***P < 0.001$. **b**, **d**, Statistical analyses between all groups and time points (two-sided one-way ANOVA): $P < 0.001$. **c**, **g**, **j**, **n**, Statistical analyses (paired two-sided Student's t-test): $*P < 0.05$; $**P < 0.01$; $***P < 0.001$.

of castration-resistant prostate tumours (castration-resistant phase, $t = 12$ weeks) (Fig. 1b and Extended Data Fig. 1c, d). AR target genes are downregulated in tumours in the castration-sensitive phase and upregulated in the castration-resistant phase in castrated mice compared to sham-operated mice (Fig. 1c). To assess whether castration

affects the recruitment of PMN-MDSCs in these tumours, we measured the frequency of PMN-MDSCs (CD11b^{+}Ly6G^{bright}Ly6C^{low} cells)[18] in sham-operated and castrated $Pten^{PC-/-}$ mice in a time course experiment. Notably, PMN-MDSCs number increased over time, paralleling the emergence of CRPC (Fig. 1b, d and Extended Data Figs. 1e, 2a).

Of note, PMN-MDSCs represented the major subset of immune cells that increased in *Pten*-null tumours upon castration (Fig. 1e and Extended Data Fig. 2b, c). This increase in PMN-MDSCs was validated in TRAMP-C1 and MyC-CaP castrated mice that develop CRPC within 10 days after castration (Extended Data Figs. 1f–i, 2a). Whereas PMN-MDSCs increased in castrated tumours, the frequency of tumour-infiltrating macrophages (TAMs) decreased (Fig. 1e and Extended Data Fig. 2c).

To assess whether factors secreted by MDSCs affect AR pathway signalling in prostate cancer cells, we co-cultured two mouse androgen-dependent prostate cancer cell lines, TRAMP-C1 and MyC-CaP, in the presence of conditioned medium obtained from bone marrow (BM)-derived MDSCs (Fig. 1f and Extended Data Fig. 3a, b). Notably, the conditioned medium of MDSCs sustained the proliferation and survival of cells cultured under full androgen deprivation (FAD), enhancing the transcription of AR target genes (Fig. 1g–j and Extended Data Fig. 3c–f). These results were further validated in both androgen-dependent (LNCaP and VCaP) and androgen-independent (22Rv1 and PC3) human prostate cancer cell lines cultured in the presence of conditioned medium from human BM-MDSCs (Fig. 1k, l and Extended Data Fig. 3g–i). Taken together, these data demonstrated that MDSCs can regulate, in a paracrine manner, androgen-deprivation sensitivity in prostate tumour cells. We next assessed whether depletion of MDSCs could delay the emergence of CRPC in castrated mice. We therefore treated castrated *Pten*[PC−/−] mice, TRAMP-C1 and MyC-CaP allograft mice with AZD5069, a selective CXCR2 antagonist that is under clinical evaluation (Clinical Trial NCT03177187, https://clinicaltrials.gov/ct2/show/NCT03177187). Treatment with the CXCR2 antagonist strongly reduced the tumour infiltration of PMN-MDSCs in all of the mouse models that were analysed (Extended Data Figs. 3j 4a, e). Notably, whereas *Pten*[PC−/−] castrated mice treated with the CXCR2 antagonist did not progress to CRPC, untreated mice developed CRPC four months after castration as demonstrated by the levels of AR target genes (Fig. 1m, n). This finding was also confirmed in TRAMP-C1 and MyC-CaP allograft mice, in which inhibition of MDSC recruitment in the tumour delayed the emergence of CRPC as shown by decreased tumour size and level of AR target genes in treated mice, resulting in longer survival in mice that were treated with the CXCR2 antagonist (Extended Data Fig. 4a–h). Of note, treatment with the CXCR2 antagonist did not directly affect cell proliferation and AR activity in mouse prostate tumour cells cultured in vitro in FAD (Extended Data Fig. 3k, l). To corroborate the role of MDSCs as drivers of CRPC in the human setting, we co-injected human BM-MDSCs with LNCaP cells in NOD/SCID mice, and assessed tumour growth over time in intact versus castrated hosts. In line with our previous results, the co-injection of LNCaP with human BM-MDSCs conferred resistance to castration (Extended Data Fig. 4i, j). Taken together, these data indicated that MDSCs are increased in CRPC and can promote proliferation of prostate tumour cells by sustaining AR signalling following androgen deprivation.

IL–23 drives insensitivity to androgen deprivation

To determine which MDSC-secreted factors drive castration resistance, we performed a NanoString nCounter gene expression assay in *Pten*[PC−/−] tumours from sham and castrated mice. IL-23 and one of the subunits of IL-23 receptor (IL12Rβ1) were the most upregulated genes in tumours from castrate mice compared to controls (Extended Data Fig. 5a). Of note, factors that had previously been linked to the regulation of AR pathway, such as IL-6, were not upregulated in *Pten*[PC−/−] tumours after castration[13] (Extended Data Fig. 5a). In line with this evidence, cytokine profile analysis of conditioned medium from mouse MDSCs showed that IL-23 was the most overexpressed factor produced by these cells (Extended Data Fig. 5b). Immunofluorescence and flow cytometry analyses further confirmed that tumour-infiltrating MDSCs expressed IL-23 in vivo, with PMN-MDSCs that infiltrated castration-resistant tumours expressing even higher levels of IL-23 compared to treatment-naive tumours (Fig. 2a, b). Moreover, similar to the results
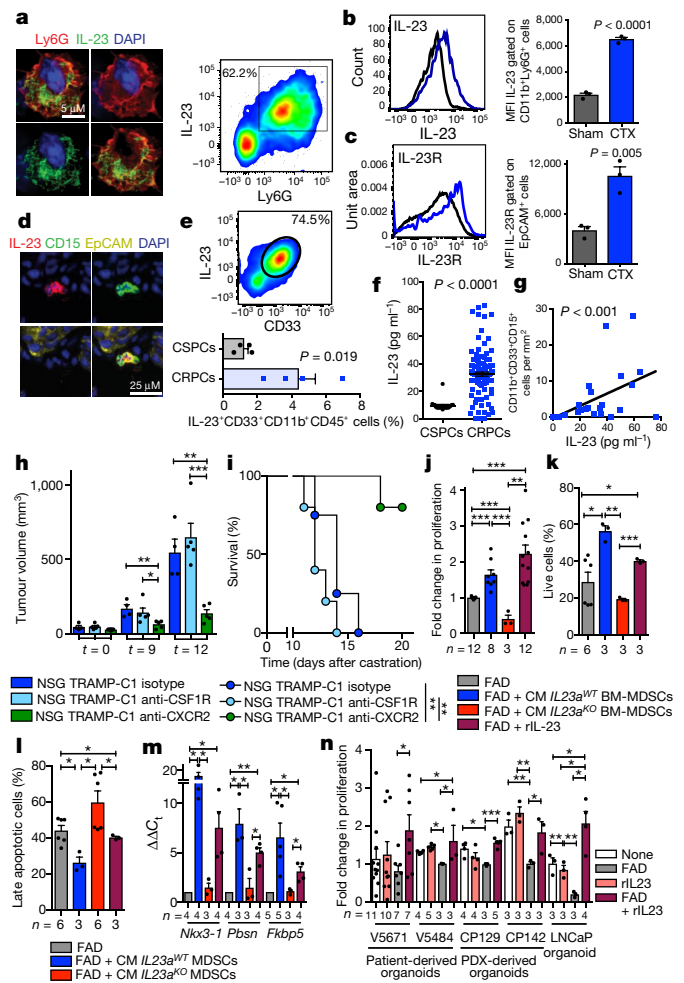

Fig. 2 | Tumour-infiltrating MDSCs produce IL-23 that drives insensitivity to androgen deprivation. a–c, Prostate tumours from *Pten*[PC−/−] sham-operated or CTX mice analysed at $t = 12$ weeks. **a,** Representative images of Ly6G+IL-23+ cells (nuclei, blue) and representative dot plot of Ly6G+IL-23+ cells gated on CD45+ cells in CTX mice. **b, c,** Representative histograms (left) and quantification (right; mean ± s.e.m.) showing the mean fluorescence intensity (MFI) of IL-23 in CD45+CD11b+Ly6G+ cells (**b**) and MFI of IL-23R gated on CD45−EpCAM+ cells (**c**). $n = 3$ biologically independent mice per group. **d,** Representative images of IL-23+, CD15+, EpCAM+ cells within the tumours of patients with CRPC. **a, d,** Data were validated in at least three experiments. **e,** CD33+IL-23+CD11b+CD45+ cells within the tumours of patients with CSPC or CRPC ($n = 4$ biologically independent patients per cohort). **f,** IL-23 levels in the plasma of patients with CSPC ($n = 20$) and CRPC ($n = 120$). **g,** Correlation analyses of the numbers of tumour-infiltrating PMN-MDSCs and plasmatic IL-23 levels in patients with CRPC ($n = 28$). Statistical analyses (negative binomial regression model): $P < 0.001$. **h, i,** Tumour progression ($t = $ days after castration) of NSG mice carrying TRAMP-C1 allografts treated with isotype control (untreated; $n = 4$), anti-CSF1R antibody ($n = 5$) or CXCR2 antagonist ($n = 5$). **h,** Average tumour volume. **i,** Survival curves reported as a Kaplan–Meier plot. Statistical analyses (log-rank (Mantel–Cox) test): **$P < 0.01$. **j,** TRAMP-C1 cell proliferation. **k,** Percentage of annexin V− and 7AAD− TRAMP-C1 cells. **l,** Percentage of annexin V+ and 7AAD+ TRAMP-C1 cells. **m,** qRT–PCR analyses of the indicated genes in TRAMP-C1 cells. **n,** Cell proliferation of 3D cultures of reported organoids. Recombinant (r) IL-23 conditions were normalized to the none or FAD treatment. **e, f, h–n,** Data are mean ± s.e.m. Specific n values of biologically independent samples are shown in **j–n**. **b, c, e, f, h–l, n,** Statistical analyses (unpaired two-sided Student's t-test). **m,** Statistical analyses (paired two-sided Student's t-test): *$P < 0.05$; **$P < 0.01$; ***$P < 0.001$.
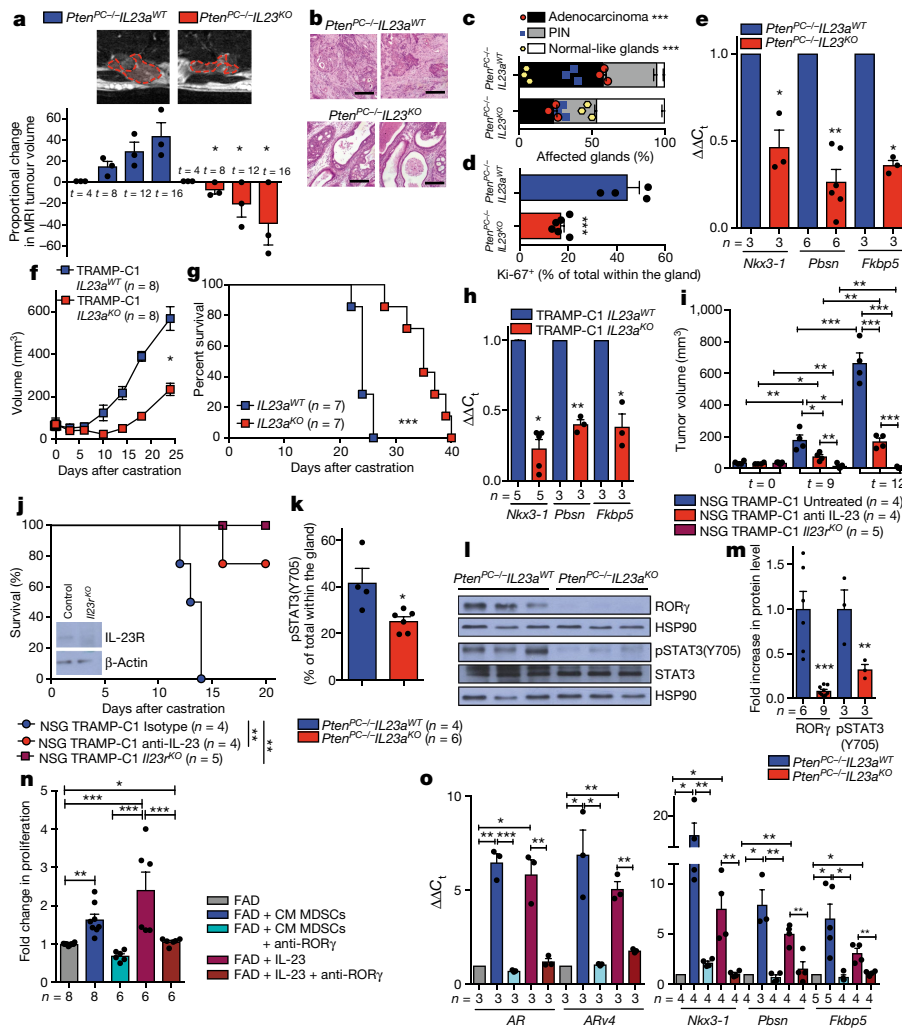
Fig. 3 | IL-23–IL-23R signalling axis regulates resistance to castration in prostate cancer in vivo and in vitro. a, Magnetic resonance imaging scans of representative $Pten^{PC-/-}Il23a^{WT}$ and $Pten^{PC-/-}Il23a^{KO}$ mice at the endpoint (top). Waterfall plot depicting proportional change in tumour response for $Pten^{PC-/-}Il23a^{WT}$ ($n = 3$) and $Pten^{PC-/-}Il23a^{KO}$ ($n = 3$) mice (bottom). Data are mean ± s.e.m. Statistical analyses: unpaired two-sided Student's t-test: *$P < 0.05$; one-way ANOVA: $P = 0.0008$. **b**, Representative haematoxylin and eosin staining at the endpoint. Scale bars, 100 μm. Data are representative of at least three biologically independent mice. **c**, Quantification of adenocarcinoma, prostatic intraepithelial neoplasia (PIN) or normal-like glands in $Pten^{PC-/-}Il23a^{WT}$ ($n = 3$) and $Pten^{PC-/-}Il23a^{KO}$ ($n = 3$) mice. **d**, Quantification of Ki-67+ cells in $Pten^{PC-/-}Il23a^{WT}$ ($n = 4$) and $Pten^{PC-/-}Il23a^{KO}$ ($n = 6$) mice. **e**, qRT–PCR analyses of the prostate tumours. **f, g**, Tumour volume and survival curves of TRAMP-C1 $Il23a^{WT}$ and TRAMP-C1 $Il23a^{KO}$ mice. **f**, Statistical analyses (unpaired two-sided Student's t-test followed by Wilcoxon signed-rank test): *$P < 0.05$. **h**, qRT–PCR analyses in the tumours of TRAMP-C1 $Il23a^{WT}$ or TRAMP-C1 $Il23a^{KO}$ mice.

i, j, NSG males challenged with TRAMP-C1 or TRAMP-C1 $Il23r^{KO}$ cells after CTX were treated with isotype control (untreated) or anti-IL-23 antibody and monitored for tumour progression (**i**) and survival (**j**). Western blot of IL-23R in TRAMP-C1 (control) or TRAMP-C1 $Il23r^{KO}$ cells is shown in the inset (performed at least twice). **g, j**, Statistical analyses (log-rank (Mantel–Cox) test): **$P < 0.01$; ***$P < 0.001$. **k**, Quantification of pSTAT3(Y705)+ cells in $Pten^{PC-/-}Il23a^{WT}$ ($n = 4$) and $Pten^{PC-/-}Il23a^{KO}$ ($n = 6$) mice. **l, m**, Western blot (**l**) and quantification (**m**) of RORγ, pSTAT3(Y705) and total STAT3 levels in prostate tumours. **n**, TRAMP-C1 cell proliferation. **o**, qRT–PCR analyses in TRAMP-C1 cells. **c, d, k**, Data are mean ± s.e.m. of one tumour per mouse (mean of three sections per tumour, ≥3 fields per section). **e–k, m–o**, Data are reported as mean ± s.e.m. Specific n values of biologically independent mice (**i–k**) and biological independent samples (**m–o**) are shown. **c, d, i, k, m, n**, Statistical analyses (unpaired two-sided Student's t-test). **e, h, o**, Statistical analyses (paired two-sided Student's t-test): *$P < 0.05$; **$P < 0.01$; ***$P < 0.001$.

found in mice, PMN-MDSCs that infiltrated tumour biopsies from patients with CRPC expressed IL-23 (Fig. 2d, e and Extended Data Fig. 6a). In addition, the frequency of IL-23-producing tumour-infiltrating PMN-MDSCs was higher in CRPC biopsies than in CSPC biopsies (Fig. 2e). Notably, expression of CXCL5, a chemokine that stimulates chemotaxis of myeloid cells through CXCR2[23], was strongly upregulated in castrated tumours compared to controls (Extended Data Fig. 5a, c, d). This, together with the finding that CXCR2 inhibition efficiently decreases the recruitment of MDSCs in castrated mice, indicates that CXCL5 is a major regulator of MDSC recruitment in CRPC.

We next assessed the levels of the IL-23 receptor (IL-23R) in tumours from sham and castrated $Pten^{PC-/-}$ mice, and found that IL-23R levels

increased in tumour cells following castration (Fig. 2c). This was further validated in TRAMP-C1 cells cultured in androgen-deprived conditions in vitro (Extended Data Fig. 5e, f). Furthermore, plasma levels of IL-23 in patients with CRPC were substantially higher than in patients with CSPC (Fig. 2f and Extended Data Fig. 5g) and statistically correlated with tumour-infiltrating PMN-MDSC counts (EpCAM−CD11b+CD33+CD15+ cells; Fig. 2g) but not with other myeloid cell population counts (CD11b+CD15− cells; Extended Data Fig. 6b). Overall, these data demonstrate that IL-23 is increased in both mouse and human CRPCs, with IL-23 levels correlating with the number of tumour-infiltrating PMN-MDSCs. Overall, tumour biopsies from patients with CRPC also had much higher $IL23A$ (which
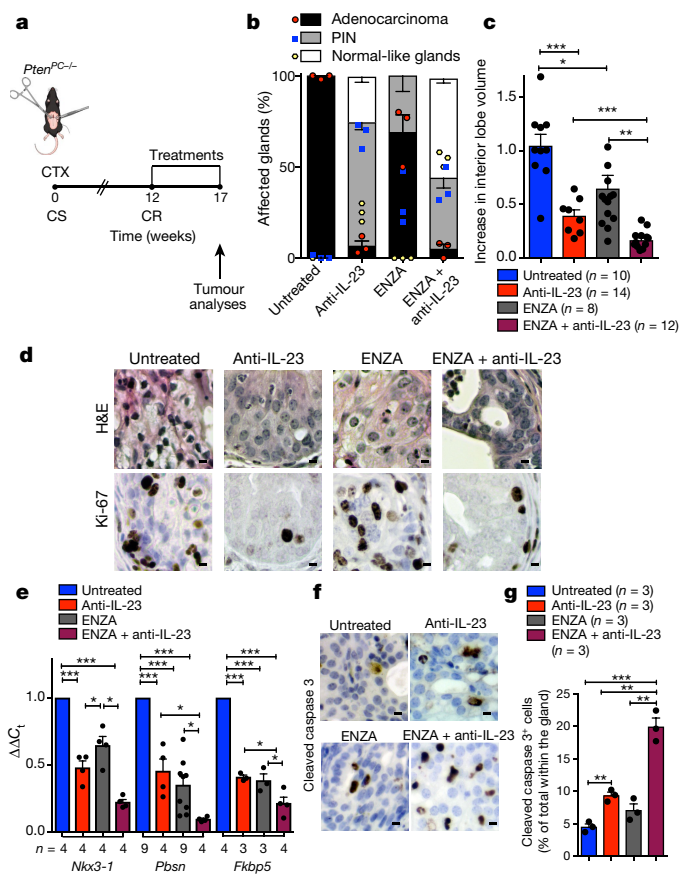
Fig. 4 | IL-23 inhibition improves ENZA efficacy in vivo.
a, $Pten^{PC-/-}$ mice with castration-resistant prostate cancer (12 weeks after castration) were randomly assigned to treatments in a preclinical study. Treatments: isotype control (untreated), anti-IL-23 antibody (100 ng per mouse injected intraperitoneally weekly), ENZA (30 mg kg^{-1} per day administered daily by oral gavage on a Monday to Friday schedule) and ENZA in combination with anti-IL-23 antibody (ENZA + anti-IL-23). **b**, Histological score. $n = 3$ biologically independent mice. Statistical analyses (two-way ANOVA): $P < 0.001$. **c**, Fold increase in the volume of the anterior lobe of the prostate (fold change over the untreated group). **d**, Representative haematoxylin and eosin (H&E) and Ki-67 staining in the tumours at completion of the study. Scale bars, 50 μm. **e**, qRT–PCR analyses of the indicated genes in the prostate tumours of CTX $Pten^{PC-/-}$ mice at completion of the preclinical study. Statistical analyses (two-sided paired Student's t-test): $*P < 0.05$; $***P < 0.001$. **f**, Representative cleaved-caspase3 staining in the tumours after one week of treatments. Scale bars, 50 μm. **g**, Quantification of cleaved-caspase 3 (percentage of the total number of cells within the glands). **d**, **f**, Data are representative of at least three biologically independent mice. **b**, **g**, Data are mean ± s.e.m. of one tumour per mouse (mean of three sections per tumour, three or more fields per section). **b**, **c**, **e**, **g**, Data are mean ± s.e.m. Specific n values of biological independent mice are shown in **c**, **e**, **g**. **c**, **e**, **g**, Statistical analyses (unpaired two-sided Student's t-test): NS, not significant; $*P < 0.05$; $**P < 0.01$; $***P < 0.001$.

encodes IL-23) and *IL23R* mRNA levels than treatment-naive patients (Extended Data Fig. 6c, d) and *IL23A* mRNA levels were linked to MDSC-associated mRNA levels in biopsies from patients with CRPC (Extended Data Fig. 6e, f).

In line with this evidence, the primary source of IL-23 in tumours from castrated $Pten^{PC-/-}$ mice was the population of PMN-MDSCs (Extended Data Fig. 6g). Note that TAMs and epithelial tumour cells were only a small fraction of the total IL-23$^+$ cells in these tumours (Extended Data Fig. 6g). In keeping with this, IL-23 levels significantly decreased in tumours from castrated $Pten^{PC-/-}$ mice that were depleted of MDSCs (Extended Data Fig. 6h), whereas the depletion of TAMs by an CSF1R antibody[24] in mice with TRAMP-C1 allografts did not delay

the emergence of CRPC. Conversely, the reduction of PMN-MDSCs by a CXCR2 antagonist robustly delayed the emergence of CRPC (Fig. 2h, i and Extended Data Fig. 6i). Overall, therefore, IL-23 levels significantly decreased in tumours depleted of MDSCs but not of TAMs (Extended Data Fig. 6j).

To functionally validate these findings, we cultured prostate tumour cells in the presence of conditioned medium from BM-MDSCs from *Il23a* wild-type ($IL23^{WT}$ BM-MDSCs) or *Il23a* knockout mice ($IL23^{ko}$ BM-MDSCs). The conditioned medium of $IL23^{WT}$ BM-MDSCs, as well as treatment with recombinant IL-23, promoted the proliferation, survival and increased the transcription of AR target genes in prostate cancer cells kept in FAD, whereas the conditioned medium of $IL23^{KO}$ BM-MDSCs was unable to affect these parameters (Fig. 2j–m). Of note, deleting IL-23 in BM-MDSCs did not affect the levels of other secreted factors in these cells (Extended Data Fig. 7a). Indeed, $IL23^{WT}$ and $IL23^{KO}$ BM-MDSCs had equal immunosuppressive capabilities (Extended Data Fig. 7b). These results were further validated in a subset of androgen-dependent organoids that were derived from patient-derived xenografts and LNCaP cells kept in FAD and treated in the presence or absence of human recombinant IL-23 (Fig. 2n). Taken together, these findings identify IL-23 as an MDSC-secreted factor that can sustain the proliferation and survival of prostate cancer cells as well as the transcription of AR-driven target genes in prostate cancer cells cultured in FAD.

MDSCs activate the IL–23–RORγ pathway
To determine whether MDSC-derived IL-23 promotes the emergence of resistance to castration in prostate cancers in vivo, we next reconstituted lethally irradiated sham-operated or castrated $Pten^{PC-/-}$ mice with bone marrow precursors from $Il23a^{WT}$ or $Il23a^{KO}$ mice (yielding $Pten^{PC-/-}IL23^{WT}$ and $Pten^{PC-/-}Il23a^{KO}$ mice, respectively; Extended Data Fig. 8a). Mice were reconstituted with bone marrow that was deprived of T, B and natural killer (NK) cells (Extended Data Fig. 8b). The absence of IL-23 in the myeloid compartment led to a marked reduction in the tumour volume of the prostate cancers specifically in castrated $Pten^{PC-/-}$ mice (Fig. 3a and Extended Data Fig. 8c), with normalization of glands that are affected by prostate cancer and a major reduction in Ki-67$^+$ cells (Fig. 3b–d and Extended Data Fig. 8d). Notably, AR target genes were robustly downregulated in prostate tumours from $Pten^{PC-/-}Il23a^{KO}$ compared to tumours from $Pten^{PC-/-}Il23a^{WT}$ mice (Fig. 3e). These data were then also validated in TRAMP-C1-allograft irradiated mice reconstituted with $Il23a^{WT}$ and $Il23a^{KO}$ bone marrow precursors (yielding TRAMP-C1 $Il23a^{WT}$ and TRAMP-C1 $Il23a^{KO}$ mice; Extended Data Fig. 9a). In TRAMP-C1 $Il23a^{KO}$ mice, the absence of IL-23 in the myeloid compartment significantly delayed the emergence of CRPC as demonstrated by decreased tumour size and tumour cell proliferation as well as reduced AR-driven target gene expression and significantly increased survival of the TRAMP-C1 $Il23a^{KO}$ mice (Fig. 3f–h and Extended Data Fig. 9b, c). Reconstitution with $Il23a^{KO}$ bone marrow did not alter the recruitment of MDSCs into the tumours and spleens of reconstituted mice (Extended Data Fig. 9d, e). Of note, treatment with anti-IL-23 antibodies or genetic inactivation of IL-23R in NOD/SCID/γ (NSG) TRAMP-C1 allografts confirmed these results (Fig. 3i, j), demonstrating that IL-23 directly promotes resistance to castration in prostate cancer by binding to IL-23R that are present on tumour cells.

IL-23 has been reported to regulate the activation of STAT3–RORγ expression in naive CD4 T cells[25–27]; both STAT3 and RORγ can affect AR signalling in prostate cancer[28,29]. We therefore evaluated whether IL-23 secreted by MDSCs affected the STAT3–RORγ signalling axis in prostate cancer in a non-cell autonomous manner. Inactivation of IL-23 in the myeloid compartment of castrated $Pten^{PC-/-}$ mice significantly decreased overall tumour levels of phosphorylated (p)STAT3 and RORγ in vivo (Fig. 3k–m and Extended Data Fig. 8d); this was also the case in the TRAMP-C1 model (Extended Data Fig. 9f–h). RORγ inhibition in vitro also abrogated the proliferative advantage conferred by conditioned medium from MDSCs or IL-23 treatment in TRAMP-C1

cells kept in FAD, and inhibited the transcription of the full-length form of the AR and its constitutively active splice variant (ARv4) as well as downstream AR target genes (Fig. 3n, o). Taken together, these data demonstrate that IL-23 released by MDSCs into the tumour microenvironment acts directly on the pSTAT3–RORγ signalling axis to drive the transcription of AR and its splice variant and downstream target genes, thus favouring the proliferation and survival of the prostate cancer cells in androgen-ablation conditions.

IL–23 targeting improves the efficacy of ADT

To evaluate the therapeutic relevance of our findings, we next assessed whether IL-23 inhibition by antibody blockade could reverse resistance to castration in prostate cancer in $Pten^{PC-/-}$ mice. Because anti-IL-23 antibodies are currently being evaluated in clinical trials for the treatment of autoimmune diseases[30], including psoriasis and are clinically well-tolerated[31], we treated mice carrying $Pten^{PC-/-}$ tumours that had become resistant to surgical castration with an anti-IL-23 antibody in combination with the AR antagonist enzalutamide (ENZA; Fig. 4a). ENZA is a standard treatment for patients with CRPC after primary ADT[2,32]. Our preclinical study showed that anti-IL-23 increased the efficacy of ENZA (Fig. 4b, c); in mice treated with anti-IL-23 and ENZA, we observed a normalization of prostate glands that were affected by cancer (Fig. 4b and Extended Data Fig. 10a), with decreased tumour volume (Fig. 4c) and proliferation (Extended Data Fig. 10a, b), whereas in mice that were treated with ENZA, alone the treatment was ineffective. Combined anti-IL-23 and ENZA were associated with a robust inhibition of the AR activity and induction of apoptosis of the tumour cells (Fig. 4e–g). Taken together, these data demonstrate that anti-IL-23 treatment can reverse resistance to castration in prostate cancer and enhance the efficacy of ENZA.

Discussion

Our study has identified IL-23 production by MDSCs as a driver of CRPC and adds novel mechanistic insights on how prostate cancers can become insensitive to androgen deprivation and AR blockade. We also report on a different role for MDSCs in cancer, describing an unexpected function for this immune subset. Previous data demonstrated that MDSCs can support tumorigenesis in many cancers through different mechanisms[15,17,18], with preclinical studies indicating that the inactivation of MDSCs increased immune-checkpoint blockade efficacy in CRPC models[16]. IL-23 has also been previously implicated in cancer progression in the context of a different tumour type as a regulator of the pro-tumour immune response[33–35]. However, to our knowledge, the discovery described here, that IL-23 produced by MDSCs regulates resistance to castration in prostate cancer by sustaining AR signalling, was previously unknown, and adds novel mechanistic insights on how these immune cells support tumorigenesis. This work also shows that inhibition of IL-23 can reverse ADT resistance in men suffering from advanced prostate cancer (Extended Data Fig. 10c).

In conclusion, we describe an alternative immunotherapeutic strategy for treating advanced prostate cancer that, unlike most other treatments, is not focused on re-activating the function of cytotoxic T lymphocytes against tumour cells. Immunotherapeutic strategies that reactivate cytotoxic T cells by immune-checkpoint blockade have been, to date, only active against a small subset of prostate cancers that are characterized by DNA-repair defects and higher neoantigen loads with increased infiltration of T lymphocytes[36,37]. Our results demonstrate, on the other hand, that MDSCs are a major player in the endocrine resistance in prostate cancer and that immunotherapies that target the blockade of either MDSC recruitment into tumour, or the direct inhibition of IL-23 can be effective therapeutic strategies for patients that have these lethal and common diseases. Because anti-IL-23 antibodies have been well-tolerated in clinical trials involving patients with autoimmune diseases[30], these deserve to be clinically evaluated in men that have lethal prostate cancer. We envision that this immunotherapeutic strategy targeting paracrine IL-23 in combination with established endocrine anticancer treatments is highly likely to improve treatment outcome for this common male cancers.

Online content

Any Methods, including any statements of data availability and Nature Research reporting summaries, along with any additional references and Source Data files, are available in the online version of the paper at https://doi.org/10.1038/s41586-018-0266-0.

1. Torre, L. A. et al. Global cancer statistics, 2012. *CA Cancer J. Clin.* **65**, 87–108 (2015).
2. Watson, P. A., Arora, V. K. & Sawyers, C. L. Emerging mechanisms of resistance to androgen receptor inhibitors in prostate cancer. *Nat. Rev. Cancer* **15**, 701–711 (2015).
3. Bianchini, D. et al. Antitumour activity of enzalutamide (MDV3100) in patients with metastatic castration-resistant prostate cancer (CRPC) pre-treated with docetaxel and abiraterone. *Eur. J. Cancer* **50**, 78–84 (2014).
4. Zhang, T. et al. Exploring the clinical benefit of docetaxel or enzalutamide after disease progression during abiraterone acetate and prednisone treatment in men with metastatic castration-resistant prostate cancer. *Clin. Genitourin. Cancer* **13**, 392–399 (2015).
5. Badrising, S. et al. Clinical activity and tolerability of enzalutamide (MDV3100) in patients with metastatic, castration-resistant prostate cancer who progress after docetaxel and abiraterone treatment. *Cancer* **120**, 968–975 (2014).
6. Noonan, K. L. et al. Clinical activity of abiraterone acetate in patients with metastatic castration-resistant prostate cancer progressing after enzalutamide. *Ann. Oncol.* **24**, 1802–1807 (2013).
7. Schrader, A. J. et al. Enzalutamide in castration-resistant prostate cancer patients progressing after docetaxel and abiraterone. *Eur. Urol.* **65**, 30–36 (2014).
8. Sartor, O. & de Bono, J. S. Metastatic prostate cancer. *N. Engl. J. Med.* **378**, 645–657 (2018).
9. Karantanos, T., Corn, P. G. & Thompson, T. C. Prostate cancer progression after androgen deprivation therapy: mechanisms of castrate resistance and novel therapeutic approaches. *Oncogene* **32**, 5501–5511 (2013).
10. Carver, B. S. et al. Reciprocal feedback regulation of PI3K and androgen receptor signaling in PTEN-deficient prostate cancer. *Cancer Cell* **19**, 575–586 (2011).
11. Quail, D. F. & Joyce, J. A. Microenvironmental regulation of tumor progression and metastasis. *Nat. Med.* **19**, 1423–1437 (2013).
12. Ammirante, M., Luo, J. L., Grivennikov, S., Nedospasov, S. & Karin, M. B-cell-derived lymphotoxin promotes castration-resistant prostate cancer. *Nature* **464**, 302–305 (2010).
13. Lee, G. T. et al. Bone morphogenetic protein-6 induces castration resistance in prostate cancer cells through tumor infiltrating macrophages. *Cancer Sci.* **104**, 1027–1032 (2013).
14. Toso, A. et al. Enhancing chemotherapy efficacy in *Pten*-deficient prostate tumors by activating the senescence-associated antitumor immunity. *Cell Rep.* **9**, 75–89 (2014).
15. Di Mitri, D. et al. Tumour-infiltrating Gr-1+ myeloid cells antagonize senescence in cancer. *Nature* **515**, 134–137 (2014).
16. Lu, X. et al. Effective combinatorial immunotherapy for castration-resistant prostate cancer. *Nature* **543**, 728–732 (2017).
17. Gabrilovich, D. I. & Nagaraj, S. Myeloid-derived suppressor cells as regulators of the immune system. *Nat. Rev. Immunol.* **9**, 162–174 (2009).
18. Bronte, V. et al. Recommendations for myeloid-derived suppressor cell nomenclature and characterization standards. *Nat. Commun.* **7**, 12150 (2016).
19. Hossain, D. M. et al. TLR9-targeted STAT3 silencing abrogates immunosuppressive activity of myeloid-derived suppressor cells from prostate cancer patients. *Clin. Cancer Res.* **21**, 3771–3782 (2015).
20. Mehra, N. et al. Myeloid-derived suppressor cells (MDSCs) in metastatic castration-resistant prostate cancer (CRPC) patients (PTS). *Ann. Oncol.* **27**, 757P (2016).
21. Murdoch, C., Muthana, M., Coffelt, S. B. & Lewis, C. E. The role of myeloid cells in the promotion of tumour angiogenesis. *Nat. Rev. Cancer* **8**, 618–631 (2008).
22. Lunardi, A. et al. A co-clinical approach identifies mechanisms and potential therapies for androgen deprivation resistance in prostate cancer. *Nat. Genet.* **45**, 747–755 (2013).
23. Bezzi, M. et al. Diverse genetic-driven immune landscapes dictate tumor progression through distinct mechanisms. *Nat. Med.* **24**, 165–175 (2018).
24. Gordon, S. R. et al. PD-1 expression by tumour-associated macrophages inhibits phagocytosis and tumour immunity. *Nature* **545**, 495–499 (2017).
25. Durant, L. et al. Diverse targets of the transcription factor STAT3 contribute to T cell pathogenicity and homeostasis. *Immunity* **32**, 605–615 (2010).
26. Kastelein, R. A., Hunter, C. A. & Cua, D. J. Discovery and biology of IL-23 and IL-27: related but functionally distinct regulators of inflammation. *Annu. Rev. Immunol.* **25**, 221–242 (2007).
27. Zhou, L. et al. IL-6 programs T(H)-17 cell differentiation by promoting sequential engagement of the IL-21 and IL-23 pathways. *Nat. Immunol.* **8**, 967–974 (2007).
28. Chen, T., Wang, L. H. & Farrar, W. L. Interleukin 6 activates androgen receptor-mediated gene expression through a signal transducer and activator of

transcription 3-dependent pathway in LNCaP prostate cancer cells. *Cancer Res.* **60**, 2132–2135 (2000).

29. Wang, J. J. et al. ROR-γ drives androgen receptor expression and represents a therapeutic target in castration-resistant prostate cancer. *Nat. Med.* **22**, 488–496 (2016).

30. Campa, M., Mansouri, B., Warren, R. B. & Menter, A. A review of biologic therapies targeting IL-23 and IL-17 for use in moderate-to-severe plaque psoriasis. *Dermatol. Ther. (Heidelb.)* **6**, 1–12 (2016).

31. Gordon, K. B. et al. A phase 2 trial of guselkumab versus adalimumab for plaque psoriasis. *N. Engl. J. Med.* **373**, 136–144 (2015).

32. Moreira, R. B. et al. Differential side effects profile in patients with mCRPC treated with abiraterone or enzalutamide: a meta-analysis of randomized controlled trials. *Oncotarget* **8**, 84572–84578 (2017).

33. Gangemi, S. et al. Clinical significance of circulating interleukin-23 as a prognostic factor in breast cancer patients. *J. Cell. Biochem.* **113**, 2122–2125 (2012).

34. Grivennikov, S. I. et al. Adenoma-linked barrier defects and microbial products drive IL-23/IL-17-mediated tumour growth. *Nature* **491**, 254–258 (2012).

35. Teng, M. W. L. et al. IL-23 suppresses innate immune response independently of IL-17A during carcinogenesis and metastasis. *Proc. Natl Acad. Sci. USA* **107**, 8328–8333 (2010).

36. Chen, D. S. & Mellman, I. Elements of cancer immunity and the cancer-immune set point. *Nature* **541**, 321–330 (2017).

37. Graff, J. N. et al. Early evidence of anti-PD-1 activity in enzalutamide-resistant prostate cancer. *Oncotarget* **7**, 52810–52817 (2016).

Reviewer information *Nature* thanks N. Brennen, D. Gabrilovich, M. Galsky and the other anonymous reviewer(s) for their contribution to the peer review of this work.

Author contributions A.A. and A.C. conceived and designed the project. A.C., C.S., E.Z. and M.M. performed experiments. V.G. performed experiments with human organoids. D.D.M., M.C. and A.N. established and carried out fluorescence microscopy. A.R. checked the quality of the RNA and performed NanoString. D.D. performed statistical analyses of multiplex immunofluorescence in human tissue sections. W.Y. performed bioinformatic analyses. G.D.B. performed surgical castration or sham operation of all animals. M.L. performed immunohistochemical experiments and analysis. A.S., M.B.L., S.S., A.F., A.B., R.L., C.A.B. and T.P.-G. selected and provided human samples. D.N.-R. reviewed tissue segmentation, cell segmentation and phenotype determination maps of tissue sections. E.P. took care of genotyping the animals. S.B. provided the AZD5069 compound. A.E. performed MRI analyses and analysed the results. J.d.B. supervised human experiments and interpreted the data. A.C. and A.A. interpreted the data and wrote the paper.

Competing interests S.B. is affiliated to IMED Oncology AstraZeneca, Li Ka Shing Centre, Cambridge, UK and provided the AZD5069 compound. The other authors declare no competing interests.

Additional information
Extended data is available for this paper at https://doi.org/10.1038/s41586-018-0266-0.
Supplementary information is available for this paper at https://doi.org/10.1038/s41586-018-0266-0.
Reprints and permissions information is available at http://www.nature.com/reprints.
Correspondence and requests for materials should be addressed to A.A.
Publisher's note: Springer Nature remains neutral with regard to jurisdictional claims in published maps and institutional affiliations.

METHODS

Animals. All mice were maintained under specific pathogen-free conditions in the IRB facility and experiments were performed according to national guidelines and regulations. All animal experiments were approved by the local ethics committee (TI13/2015 and TI04/2017). Male C57BL/6, FVB, NSG, NOD/SCID mice 6–8 weeks of age were purchased from Jackson Laboratories (Envigo) and acclimatized for at least a week before experiments. Male C57BL/6 IL-23p19KO ($Il23a^{KO}$) mice[27] were provided by F. Sallusto (IRB, Bellinzona) and used at 8 weeks of age. Male $Pten^{PC-/-}$ mice were generated and genotyped as previously described[17]. Female $Pten^{loxP/loxP}$ mice were crossed with male PB^{cre4} transgenic mice and genotyped for Cre using the following primers: primer 1 (5′-AAAAGTTCCCCTGCTGATGATTTGT-3′) and primer 2 (5′-TGTTTTTGACCAATTAAAGTAGGCTGTG-3′) for $PTEN^{loxP/loxP}$; primer 1 (5′-TGATGGACATGTTCAGGGATC-3′) and primer 2 (5′-CAGCCACC AGCTTGCATGA-3′) for PB^{cre}. Surgical castration was performed under anaesthesia with isoflurane. Male $Pten^{PC-/-}$ mice were 9–10 weeks old at the time of castration. Mice were monitored postoperatively for recovery from anaesthesia and checked daily for four days postoperatively. Surgical skin clips were removed on postoperative day 5. Mice undergoing treatment were administered control vehicle or therapeutic doses of the appropriate agents. Any mouse that showed signs of distress or lost more than 15% of their initial weight during treatment was euthanized by CO_2 asphyxiation. At the completion of study, mice were euthanized by CO_2 asphyxiation and tissue was collected for histology, mRNA and protein analysis and single-cell suspensions for flow cytometry. For allograft experiments, 2.5×10^6 TRAMP-C1 cells, 2.5×10^6 TRAMP-C1 $Il23r^{KO}$ cells or 2×10^6 MyC-CaP cells were injected subcutaneously into the flank of male C57BL/6, C57BL/6 or FVB mice, respectively. For xenograft experiments 3×10^6 LNCaP cells were suspended with or without 3×10^6 human BM-MDSCs in a total volume of 100 μl PBS and Matrigel (1:1) and implanted subcutaneously into the flank of NOD/SCID mice. When tumours were approximately 100 mm³, mice were randomized to the treatment groups. Tumour growth was monitored daily by measuring the tumour size with calliper. The tumour volume was estimated by calculating $4/3\pi(R_1 \times R_2 \times R_3)$, where R_1 and R_2 are the longitudinal and lateral radii and R_3 is the thickness of the tumour that protrudes from the surface of normal skin. Animals were euthanized when the tumour reached approximately 600 mm³. The local ethics committee approved the conduction of the in vivo experiments with maximal tumour sizes of 1,000 mm³.

Treatments. The CXCR2 antagonist (AZD5069; Astrazeneca) was administered with daily intraperitoneal injections at a final concentration of 100 mg kg⁻¹ on a Monday through Friday schedule. Control animals received vehicle. Enzalutamide (APExBio) was administered daily by oral gavage with a dose of 30 mg kg⁻¹ per day on a Monday through Friday schedule. Rat anti-IL-23 antibody (100 ng per mouse; G23-8; IgG1, kappa; eBioscience) or rat IgG1 isotype control (eBioscience) was administered weekly via intraperitoneal injection. For in vivo depletion of macrophages, mice were treated with 400 μg anti-CSF1R (clone BE0213, BioXCell; on Mondays, Wednesdays and Fridays).

Cell lines. The TRAMP-C1, MYC-CaP, LNCaP, VCaP, 22Rv1 and PC3 cell lines were obtained from the ATCC and no other authentication method was performed. The TRAMP-C1 $Il23r^{KO}$ cell line was generated in the laboratory with CRISPR–Cas9 methodology and authenticated by western blotting and FACS for the deletion of IL-23R. All cell lines were regularly tested for mycoplasma (MycoAlert Mycoplasma Detection kit).

Bone marrow reconstitution. Bone marrow was flushed from the femurs of male C57BL/6 or IL-23p19ko mice under sterile conditions with RPMI 1640 using a 21-gauge needle. Mononuclear cells were filtered, collected and checked for viability using trypan blue. Before transplantation, bone marrow-derived cells were depleted of CD3⁺ T cells, NK1.1⁺ NK cells and CD19⁺ B cells by magnetic bead separation (STEMCELL Technologies). Recipient C57BL/6 or $Pten^{PC-/-}$ mice were lethally irradiated (900 rad) and transplanted 2 h later with 10⁷ viable bone marrow cells from either C57BL/6 or IL-23p19ko mice. For TRAMP-C1 allografts, the animals were challenged subcutaneously with TRAMP-C1 cells upon bone marrow engraftment. When tumours reached approximately 100 mm³, mice were surgically castrated and monitored for tumour progression.

Magnetic resonance imaging. Magnetic resonance imaging (MRI) was performed on castrated $Pten^{PC-/-}$ mice 0, 4, 8, 12 and 16 weeks after surgical castration or on CTX $Pten^{PC-/-}Il23a^{WT}$ and CTX $Pten^{PC-/-}Il23a^{KO}$ mice 4, 8, 12 and 16 weeks after surgical castration using a 7T preclinical magnetic resonance scanner (Bruker, BioSpec 70/30 USR, Paravision 5.1) equipped with 450/675 mT/m gradients (slew-rate: 3400–4500 T/m/s; rise-time 140 μs) and a mouse body volume coil. Mice were under general anaesthesia with 1.5–2% isoflurane vaporized in 100% oxygen (flow: 1 l min⁻¹). Breathing and body temperature were monitored (SA Instruments, Inc.) and maintained around 30 breaths per minute and 37 °C, respectively. MRI studies included a Rapid Acquisition with Relaxation Enhancement (RARE) High-Resolution T2-weighted (T2w) sequence with fat suppression

acquired in the axial plane (TR = 3,800 ms, TE = 45 ms, FOV = 27 mm × 18 mm, spatial resolution = 0.094 × 0.087 mm² per pixel, scan time = 8 min, thickness = 0.70 mm, 26 slices) and in the coronal plane (TR = 3,500 ms, TE = 38 ms, FOV = 33 mm × 33 mm, spatial resolution = 0.129 × 0,129 mm² per pixel, scan time = 5 min, thickness = 0.60 mm, 20 slices). Images were analysed using NIH software MIPAV (version 7.4.0). The circumference of the whole prostate was outlined on each RARE T2w axial slice containing identifiable prostate and the number of bounded pixels in each slice was computed and added to yield the prostate volume. Coronal T2w images were used for the accurate identification of the basal and apical limits of the prostate.

Differentiation of BM-MDSCs in vitro. Mouse BM-MDSCs were differentiated in vitro as previously described[38]. In brief, bone marrow precursors were flushed from the femurs of C57BL/6 or IL-23p19ko mice with RPMI 1640 medium. The cell pellet was resuspended (one femur in 10 ml) in RPMI 1640 containing 10% heat-inactivated FBS and the cells were cultured in vitro in the presence of 40 ng ml⁻¹ GM-CSF and 40 ng ml⁻¹ IL-6. On day 4, the cells were washed and resuspended with RPMI 1640 containing 10% heat-inactivated charcoal-stripped FBS. The day after the cells were stimulated with PMA and ionomycin and after 4h the supernatant was collected and stored at −80 °C. Analysis of soluble molecules was conducted with Mouse CytokineMAP B version 1.0 (Rules Based Medicine).

Human BM-MDSCs were differentiated in vitro by seeding 10⁶ per ml bone marrow precursors in T25 flasks with RPMI 1640 containing 10% heat-inactivated FBS in the presence of 10 ng ml⁻¹ GM-CSF and 10 ng ml⁻¹ IL-6 for seven days[39]. Complete medium was changed when required. After seven days, the cells were analysed by flow cytometry for CD11b, CD33, CD15, HLA-DR expression and when the CD11b⁺CD33⁺CD15⁺HLA-DR⁻ population was higher than 80%, the cells were re-suspended in RPMI 1640 containing 10% heat-inactivated charcoal-stripped FBS and after one day stimulated with PMA and ionomycin for 5 h. The supernatant was then collected and stored at −80 °C.

In vitro culture experiments. Prostate cancer cell lines were starved in charcoal-stripped FBS medium for 72 h and then cultured with RPMI 1640 containing 10% heat-inactivated FBS (normal medium) or kept in full androgen-deprivation medium (FAD; RPMI 1640 containing 10% heat-inactivated charcoal-stripped FBS plus ENZA 10 μM). Then, the cells were stimulated with or without conditioned medium obtained from activated BM-MDSCs, or recombinant IL-23 (100 ng ml⁻¹; R&D Systems), with or without ROR-γ antibody (5 μM; SR2211, Calbiochem). Then the cells were analysed using the crystal violet assay (after 72 h of culture, fold change over the FAD condition), stained with annexin V and 7AAD (after 72 h of culture) or collected for RNA extraction (after 24 h of culture; fold change over the FAD condition).

Analyses of *IL23A* and *IL23R* mRNA expression in clinical tumours. CSPC RNA-sequencing data for 550 patients was downloaded from the UCSC Cancer Browser (https://genome-cancer.ucsc.edu/proj/site/hgHeatmap/). Metastatic castration resistant prostate cancer (mCRPC) RNA-sequencing data for 122 mCRPC patients was generated as part of the SU2C effort[40]. The paired-end transcriptome sequencing reads were aligned to the human reference genome (GRCh37/hg19) using TopHat2[41] (version 2.1.0). Gene expression, as fragments per kilobase of exon per million fragments mapped (FPKM; normalized measure of gene expression), was calculated using Cufflinks[42]. MDSC marker (CD11b, CD33, CD14 and CD15) positive and negative was defined by the high and low quantiles of RNA expression of each transcript and *IL23A* and *IL23R* expression level in each biomarker groups were compared by Student's *t*-test. In order to compare gene expression level between TCGA and SU2C with minimum experimental bias, we included only genes expressed in both TCGA and SU2C with median expression level (FPKM) >0. The gene expression levels in each sample were quantile-normalized, and *IL23A* expression levels in CSPC and CRPC were compared using a Student's *t*-test.

Human organoids. Organoids were grown in 3D Matrigel (356231, Corning) under prostate epithelial conditions[43]. Cell viability was measured using 3D CellTiter-Glo 3D reagent (G9681, Promega) by quantifying metabolically active cells releasing ATP. Cell line-derived organoids were plated at a density of 2,000 cells per well in 96-well optical plates (3610, Corning) embedded in Matrigel as hanging drops (5 μl per well). Cells were treated with recombinant IL-23 (300-01A, PeproTech) at 100 ng ml⁻¹ or culture with ENZA (10 μM) with or without recombinant IL-23. Luminescence measurements were performed after seven days in culture. Each IL-23 condition was normalized to its experimental control.

Characterization of the immune tumour microenvironment. Tumours were disaggregated and digested in collagenase D and DNase for 30 min at 37 °C to obtain a single-cell suspension. For intracellular cytokine detection, cells were stimulated for 5 h with PMA and ionomycin plus Golgi Plug. After neutralization of unspecific binding with CD16/CD32 antibody (clone 93), single-cell suspensions were stained with specific monoclonal antibodies (primary antibodies directly conjugated) to assess the phenotype and diluted 1:200. The antibodies used were: CD45 (clone 30-F11, lot no. B235438); Ly-6G (clone 1A8, lot no. B194432); Ly6C (clone HK1.4, lot no. B243043), CD11b (clone M1/70, lot no. B233927); F4/80 (clone

BM8, lot no. 4305911), CD206 (clone C068C2, lot no. B230155), CD11c (clone N418, lot no. B226270), B220 (clone RA3-6B2, lot no. B210434), CD3 (clone 145-2C11, lot no. B241616), CD8 (clone 53-6.7, lot no. B193838), CD4 (clone GK1.5, lot no. B240053), NK1.1 (clone PK136, lot no. 4291566), CD90.2 (clone 30-H12, lot no. B190542), PDL1 (clone 10F.9G2, lot no. B191993), EpCAM (clone G8.8, lot no. B230070), pan-cytokeratin (clone C11, Lot. 4528S), IL-17 (clone TC11-18H10.1, lot no. B201753), IL-23p19 (clone FC23CPG, lot no. 4321359), isotype (rat IgG1, kappa, eBRG1) IL-23R (clone 12B2B64, lot no. 4321359). For flow gating, we used isotype controls of fluorescence minus one controls. All the antibodies were purchased from eBioscience or Biolegend. Samples were acquired on a BD Fortessa flow cytometer (BD Biosciences). Data were analysed using FlowJo software (TreeStar).

Immunohistochemistry and immunofluorescence of mouse tissues. For immunohistochemistry, tissues were fixed in 10% formalin (5701, ThermoScientific) and embedded in paraffin in accordance with standard procedures. Preceding immunohistochemical staining, tumour sections (4 μm) were exposed to two washes with OTTIX plus solution (X0076, Diapath) and subsequent hydration in OTTIX shaper solution (X0096, Diapath) followed by deionized water. Antigen unmasking was performed by heating sections in the respective pH solutions based on the antibodies used at 98 °C for 20 min. Subsequently the sections were blocked for peroxidases and nonspecific binding of antibodies using 3% H_2O_2 (23615.248, VWR) and Protein-Block solution (X0909, DAKO Agilent technologies), respectively, for 10 min each, split by 0.5% PBST washing. Haematoxylin and eosin staining was performed according to standard procedures. Sections were stained for anti-Ki-67 (clone SP6; Laboratory Vision Corporation), anti-pSTAT3 (Tyr705; clone D3A7; Cell Signaling). Images were obtained using objectives of 5×, 10× and 40× magnification and pixel images of 2.24 μm, 1.12 μm and 0.28 μm, respectively. All the quantifications were done using the public online software ImmunoRatio (http://153.1.200.58:8080/immunoratio/). For the immunofluorescence staining, tissue paraffin-embedded sections were stained with 4′,6-diamidine-2′-phenylindole dihydrochloride (DAPI) (70238421, Roche), anti-IL-23 (ab45420, Abcam), anti-Ly6G (RB6-8C5, GeneTex). Confocal images were obtained with the Leica TCS SP5 confocal microscope using a 10×/1.25 NA oil objective.

In vitro T cell suppression assay. In vitro suppression assays were carried out in RPMI with 10% FCS in 96-well U-bottom plates (Corning). Naive splenocytes were labelled with 5 μM CFSE (Molecular Probes) and activated in vitro with anti-CD3 and anti-CD28 beads (Invitrogen) according to the manufacturer's instructions. Conditioned medium from BM-MDSCs was added to the culture. After three days, the proliferation of CFSE-labelled $CD8^+$ T cells was analysed by BD Fortessa.

CRISPR–Cas9 transfection. TRAMP-C1 cells were grown in 75-cm² flask to 50–60% confluency in DMEM medium supplemented with 10% heat-inactivated FBS, 100 U ml^{-1} penicillin, 0.1 mg ml^{-1} streptomycin and 2 mM L-glutamine. The transfection of the *Il23r* CRISPR–Cas9 KO plasmid (Santa Cruz Biotechnology) was performed using jetPRIME transfection reagent according to the manufacturer's protocol at the 1:2 DNA:jetPRIME ratio. After 24 h of transfection, GFP-transduced cells were sorted to 99% purity and single cells were plated in 96-well plates. At day 7 after sorting, the grown cell clones were moved into 24-well plates for further expansion. The knockdown of the *Il23r* gene in each cell colony was confirmed by western blot.

NanoString. The nCounter analysis system (NanoString Technologies) was used to screen for the expression of signature genes associated with cancer–inflammation pathways. Two specific probes (capture and reporter) for each gene of interest were used. In brief, 5 μl of RNA (the concentration is higher than 25 ng μl^{-1}) was hybridized with customized Reporter CodeSet and Capture ProbeSet as Mouse PanCancer Immune Profiling Panel including 700 selected genes (NanoString Technologies) according to the manufacturer's instructions for direct labelling of mRNAs of interest with molecular barcodes without the use of reverse transcription or amplification. Total RNA was quantified by NanoDrop ND-1000 Spectrophotometer (NanoDrop Technologies, Wilming-ton, DE) and RNA quality was assessed using an Agilent 2100 Bioanalyzer (Agilent Technologies). The hybridized samples were then recovered in the NanoString Prep Station and the mRNA molecules were counted with the NanoString nCounter. For expression analysis, each sample profile was normalized to geometric mean of 20 housekeeping genes included in the panel.

Immune tumour microenvironment characterization of tumours from patients with prostate cancer. Tumours were disaggregated and digested in collagenase I and DNase for 20 min at 37 °C to obtain single-cell suspensions. For intracellular cytokine detection, cells were stimulated for 5 h with PMA and ionomycin plus Golgi Plug. Single-cell suspensions were stained with specific monoclonal antibodies diluted 1:200 (primary antibodies directly conjugated) to assess the phenotype. The antibodies used were: CD45RA (clone MEM-56, 1:50), CD33 (clone WM53), CD11b (clone ICRF44), CD15 (clone W6D3), HLA-DR (clone L243), IL-23p19 (clone 23DCDP). For flow gating, we used isotype controls of fluorescence minus one controls. All antibodies were purchased from eBioscience or Biolegend.

Samples were acquired on a BD Fortessa flow cytometer (BD Biosciences). Data were analysed using FlowJo software (TreeStar.

Protein profiling. Plasma pools of patients with CSPC or CRPC were processed as indicated in the Human XL Cytokine Array Kit (R&D Systems). Pools of tissue lysates of tumours from sham and castrated $Pten^{PC-/-}$ mice were processed as indicated in the Mouse XL Cytokine Array Kit (R&D Systems). Developed films were scanned, the obtained images were analysed using ImageJ version 1.43u and background signals were subtracted from the experimental values.

Multiplex immunofluorescence in formalin-fixed paraffin-embedded tissue section. *PMN-MDSC panel (CD15, CD11b, CD33 and EpCAM).* Multiplex immunofluorescence for CD15 (M3631, Dako, clone Carb-3), CD33 (ab11032, Abcam, clone 6C5/2), CD11b (ab52477, Abcam, clone EP1345Y) and EpCAM Alexa Fluor 647 conjugate (5447S, Cell Signaling, clone VU1D9) was performed using 4-μm sections of formalin-fixed paraffin-embedded (FFPE) prostate tumour samples by sequential staining after antigen retrieval in CC1 (pH 8.5) (950-224, Ventana) in a water bath at 98 °C for 36 min. First, mouse monoclonal (IgG1) antibody anti-CD33 (1:100 dilution), mouse monoclonal (IgM) anti-CD15 (1:200 dilution) and rabbit monoclonal (IgG) antibody anti-CD11b (1:100 dilution) were incubated for 1 h after blocking with 10% goat serum for 30 min. Slides were then incubated with goat anti-mouse IgG1 Alexa Fluor 555-conjugated (A21127, Life Technologies), goat anti-mouse IgM Alexa Fluor 488-conjugated (A21042, Life Technologies) and goat anti-rabbit IgG (H+L) Alexa Fluor 700-conjugated (A21038, Life Technologies) antibodies for 30 min. Next, tissue sections were treated with 5% mouse or rabbit normal serum for 30 min, followed by incubation with a mouse monoclonal (IgG1) anti-EpCAM antibody conjugated to Alexa Fluor 647 (dilution, 1:200) for 1 h. The samples were washed three times for 5 min with TBS Tween 0.05% between incubations. Nuclei were counterstained with DAPI (70238421, Roche) and tissue sections were mounted with ProLong Gold antifade reagent (P36930, Molecular Probes).

CD15, IL-23 and EpCAM. Immunofluorescence was performed on 4-μm FFPE tissue sections using an automated staining platform (Bond-RX, Leica Microsystems). In brief, antigen retrieval was achieved using ER1 (pH 6.0) (AR9961, Leica Biosystems) for 30 min. Sections were blocked in 10% normal goat serum for 30 min at room temperature. Primary antibodies, including mouse monoclonal (IgM) anti-CD15 (M3631, Dako, clone Carb-3, dilution 1:200), rabbit monoclonal (IgG) anti-IL-23 (ab190356, Abcam, clone EPR5585(N), dilution 1:100) and mouse monoclonal (IgG1) anti-EpCAM (2929S, Cell Signaling, clone VU1D9, dilution 1:500), were incubated for 1 h. Slides were then incubated with goat anti-rabbit (H+L) Alexa Fluor 555-conjugated (A21429, Life Technologies), goat anti-mouse IgM Alexa Fluor 488-conjugated (A21042, Life Technologies) and goat anti-mouse IgG1 Alexa Fluor 647-conjugated (A21240, Life Technologies) antibodies for 30 min. Nuclei were counterstained with DAPI (70238421, Roche) and tissue sections were mounted with ProLong Gold antifade reagent (P36930, Molecular Probes).

Microscopy and image acquisition. After staining, slides were scanned using the multi-spectral camera provided by Vectra (Perkin Elmer) system. The number of images collected per case was dependent on tumour size from minimum of 1 to a maximum of 18 (average = 12). Quantification of PMN-MDSC-like cells ($CD15^+$ $CD33^+CD11b^+$) was performed using inForm v.2.1.1 software (PerkinElmer) and the density of cells of interest are presented as the number of cells per mm². A tissue segmentation algorithm based on EpCAM positivity was used to separate tumour from adjacent stroma. The algorithm was trained to perform cell segmentation using counterstaining-based segmentation achieved with nuclear DAPI staining. Phenotype determination was based on positivity for CD15, CD33 and CD11b. Cells in tumour areas selected by the algorithm were then separated into bins as follows: $CD15^+CD33^+CD11b^+$ cells were called PMN-MDSC-like cells and $CD15^-CD11b^+$ cells were called $CD15^-CD11b^+$ cells. All tissue segmentation, cell segmentation and phenotype determination maps were reviewed by a pathologist.

Validation of antibody specificity for multiplex immunofluorescence. Immunohistochemistry was performed on 4-μm FFPE tissue sections using an automated staining platform (Bond-RX, Leica Microsystems). Optimal antibody concentrations were determined for primary antibodies against CD15 (M3631, Dako, clone Carb-3, dilution 1:200), CD33 (ab11032, Abcam, clone 6C5/2, dilution 1:100), CD11b (ab52477, Abcam, clone EP1345Y, dilution 1:100) IL-23 (ab190356, Abcam, clone EPR5585(N), dilution 1:100) and EpCAM (2929S, Cell Signaling, clone VU1D9, dilution 1:500). Antibody labelling was detected with the Bond Polymer Refine Detection Kit (DS9800, Leica Microsystems). 3,3-diaminobenzidine tetrahydroxychloride (DAB) was used as chromogen and the slides were counterstained with haematoxylin. Human control samples included colorectal specimens. In each staining batch, positive and negative controls were incubated with and without primary antibody.

RNA expression and qPCR. RNA isolation (TRIzol, Qiagen) and retro-transcription with SuperScriptIII (Invitrogen, 11752-250) were performed according to the manufacturer's instructions. qPCR reactions (Bio-Rad) were performed using

KAPA SYBR FAST qPCR green (KK4605; Applied Biosystems) and the specific primers reported below. Primer sequences were obtained from PrimerBank (http://pga.mgh.harvard.edu/primerbank/index.html) or Bio-Rad. Each expression value was normalized to *HPRT* or *GADPH* level as reference. The primer sequences used were as follows: *CXCL1* forward, 5′-CTGGGATTCACCTCAAGAACATC-3′; reverse, 5′-CAGGGTCAAGGCAAGCCTC-3′. *CXCL2* forward, 5′-GCGTCACAC TCAAGCTCTG-3′; reverse, 5′-CCAACCACCAGGCTACAGG-3′; *CXCL3* forward, 5′-ATCCCCCATGGTTCAGAAA-3′; reverse, 5′-ACCCTGCAGGAAG TGTCAAT-3′; *CXCL5* forward, 5′-GTTCCATCTCGCCATTCATGC-3′; reverse, 5′-GCGGCTATGACTGAGGAAGG-3′. *GAPDH* forward, 5′-AGGT CGGTGTGAACGGATT-3′; reverse, 5′-TGTAGACCATGTAGTTGAG-3′. *IL23p19* forward, 5′-CCAGCAGCTCTCTCGGAATC-3′; reverse, 5′-TCATATG TCCCGCTGGTGC-3′. Bio-Rad primers used were: *Hprt* PrimePCR PreAmp for SYBR Green Assay: *Hprt*, mouse qMmuCID0005679; *Ar* PrimePCR PreAmp for SYBR Green Assay: *Ar*, mouse qMmuCID0005164; *Nkx3-1* PrimePCR PreAmp for SYBR Green Assay: *Nkx3-1*, mouse qMmuCED0046482; *Pbsn* PrimePCR PreAmp for SYBR Green Assay: *Pbsn*, mouse qMmuCID0017831; *Fkbp5* PrimePCR PreAmp for SYBR Green Assay: *Fkbp5*, msouse qMmuCID0023283.

Western blot analyses and protein detection. Tissue and cell lysates were prepared with RIPA buffer ($1\times$ PBS, 1% Nonidet P40, 0.5% sodium deoxycholate, 0.1% SDS and protease inhibitor cocktail; Roche). The total protein concentration was measured using a BCA Protein Assay Kit (23225; Pierce). Equal amounts of proteins were separated by SDS–PAGE and western blotted onto a 0.45-μm nitrocellulose membrane. Membranes were blocked in 5% defatted milk or 5% BSA in Tris-buffered saline containing 0.1% Tween-20 (TBST), probed with diluted antibodies and incubated at 4°C overnight. The following primary antibodies were used: rabbit polyclonal anti-HSP90 (1:1,000 dilution, Cell Signaling), rabbit polyclonal anti-pSTAT3 (Tyr705) (1:1,000 dilution, Cell Signaling), rat monoclonal anti-RORγt (5:1,000 dilution, clone AFKJS-9, eBioscience), rabbit polyclonal anti-IL-23R (H-300) (1:1,000 dilution, Santa Cruz). After washing in TBST, the membrane was incubated with secondary antibodies that were conjugated to horseradish peroxidase (HRP) (1:5,000 dilution, Cell Signaling). The protein bands were visualized using the ECL Western Blotting Substrate (Pierce).

Samples from human prostates. Samples were acquired from patients with mCRPC, who had given their written informed consent to institutional protocols approved either by the Royal Marsden NHS Foundation Trust Hospital (London, UK) Ethics Committee (reference no. 04/Q0801/60), the IRCCS Ospedale San Raffaele (Milan, Italy) Ethics Committee (reference no. 99/INT/2004; 58/INT/2010) or the Azienda Ospedaliera di Padova (Padova, Italy) Ethics Committee (reference no. CESC/958P/2005). Human biological samples were sourced ethically and their research use was in accord with the terms of the informed consent provided. Fifty-one patients with CRPC treated at The Royal Marsden NHS Foundation Trust Hospital with sufficient formalin-fixed, paraffin-embedded, had matching CSPC and CRPC biopsies identified for multiplex immunofluorescence (see Supplementary Table 1). Four patients with CRPC, enrolled at Azienda Ospedaliera di Padova, and four patients with CSPC, enrolled at IRCCS Ospedale San Raffaele, were selected to perform the immune tumour microenvironment characterization by flow cytometry analyses. Case selection was blinded to baseline

characteristics, treatments received, clinical outcome and molecular characterization to reduce any potential selection bias. Finally, plasma from 120 patients with CRPC with sufficient samples stored (including 28 plasma samples within 40 days of CRPC biopsy) and 20 patients with CSPC were analysed for IL-23 levels.

Statistical analysis and reproducibility. Data analyses were carried out using GraphPad Prism version 7. The data are mean $\pm$ s.e.m., individual values as scatter plots with column bar graphs and were analysed using Student's *t*-tests (paired or unpaired according to the experimental setting) by a two-sided test, and, when indicated, followed by Wilcoxon signed-rank test. One-way ANOVA was used to compare three or more groups in time point analyses. Differences were considered significant when $P < 0.05$ and are indicated as not significant, $*P < 0.05$, $**P < 0.01$, $***P < 0.001$. Non-parametric tests were applied when variables were not normally distributed using the SPSS statistical software. *n* values represent biological replicates. Survival curves were compared using the log-rank test (Mantel–Cox). Because of evidence of overdispersion, tumour-infiltrating PMN-MDSC ($CD15^+CD11b^+CD33^+EpCAM^-$) and $CD15^-CD11b^+$ cells were analysed using mixed-effect negative binomial regression model (with per patient random intercept) when comparing paired biopsies, and a negative binomial regression model was used when analysing the association between CRPC biopsies and IL-23. PMN-MDSC (coefficient, 1.49; 95% confidence interval, 0.83–2.15; $P < 0.001$); $CD15^-CD11b^+$ cells (coefficient, 0.43; 95% confidence interval, 0.04–0.83; not significant ($P > 0.05$)). All statistics and reproducibility information are reported in the figure legends. For animal studies, sample size was defined on the basis of past experience with the models[15], to detect differences of 20% or greater between the groups (10% significance level and 80% power). For ethical reasons the minimum number of animals necessary to achieve the scientific objectives was used. Animals were allocated randomly to each treatment group. Different treatment groups were processed identically and animals in different treatment groups were exposed to the same environment.

Reporting summary. Further information on experimental design is available in the Nature Research Reporting Summary linked to this paper.

Data availability. Source Data for the figures and extended data figures are provided in the online version of the paper. CSPC and mCRPC tumour biopsy mRNA-seq data that support the findings of this study are available in the SU2C-PCF IDT cBioportal (http://www.cbioportal.org) and through dbGAP (https://www.ncbi.nlm.nih.gov/gap/) with the identifier phs000915.v1.p1[40].

38. Marigo, I. et al. Tumor-induced tolerance and immune suppression depend on the C/EBPβ transcription factor. *Immunity* **32**, 790–802 (2010).
39. Lechner, M. G., Liebertz, D. J. & Epstein, A. L. Characterization of cytokine-induced myeloid-derived suppressor cells from normal human peripheral blood mononuclear cells. *J. Immunol.* **185**, 2273–2284 (2010).
40. Robinson, D. et al. Integrative clinical genomics of advanced prostate cancer. *Cell* **161**, 1215–1228 (2015).
41. Kim, D. et al. TopHat2: accurate alignment of transcriptomes in the presence of insertions, deletions and gene fusions. *Genome Biol.* **14**, R36 (2013).
42. Trapnell, C. et al. Differential gene and transcript expression analysis of RNA-seq experiments with TopHat and Cufflinks. *Nat. Protoc.* **7**, 562–578 (2012).
43. Drost, J. et al. Organoid culture systems for prostate epithelial and cancer tissue. *Nat. Protoc.* **11**, 347–358 (2016).
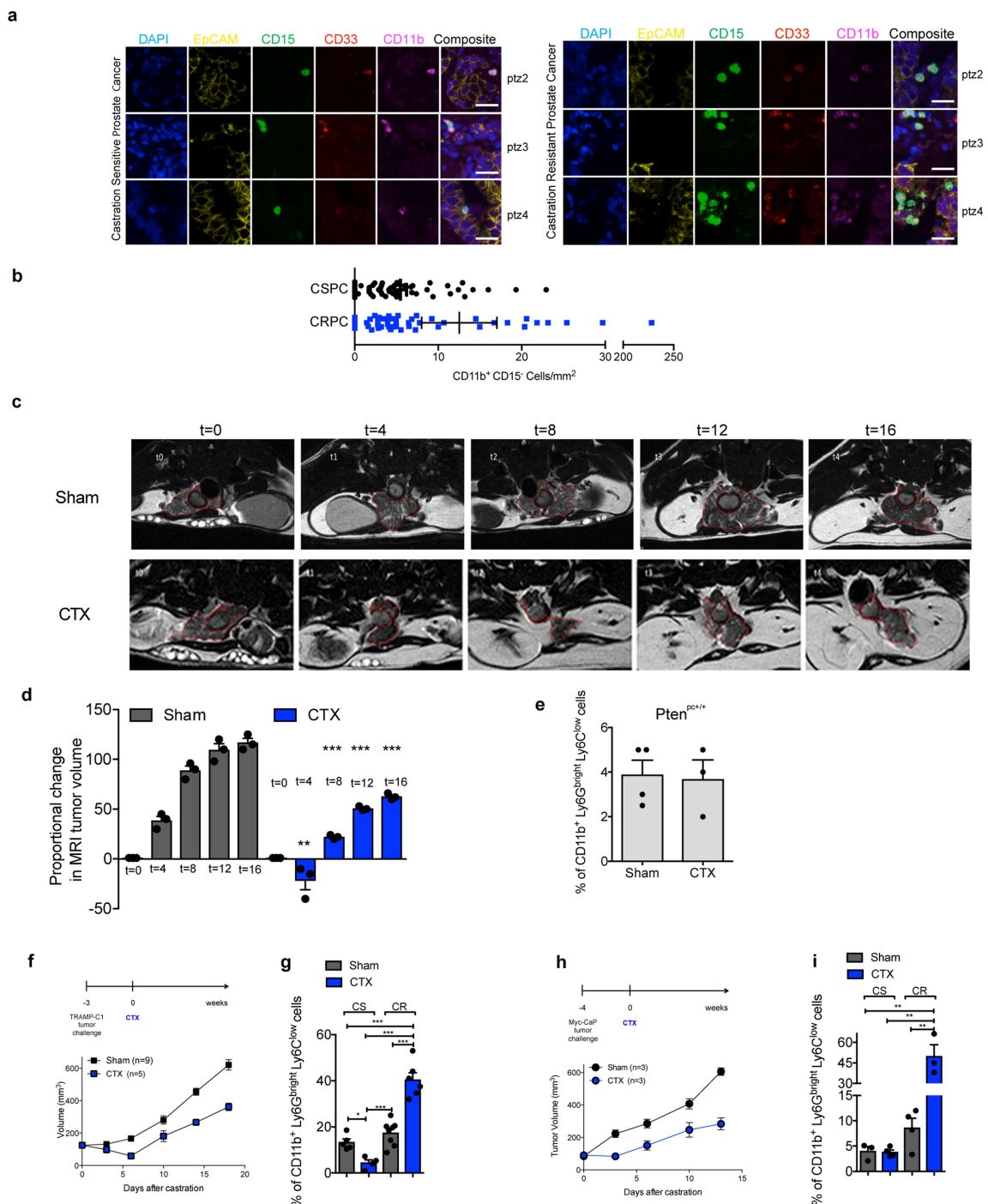
**Extended Data Fig. 1 | Multispectral images of PMN-MDSCs in human biopsies and set-up of the different CRPC mouse models.** **a**, Multispectral microscopy images (EpCAM, yellow; CD15, green; CD33, red; CD11b, pink) of castration-sensitive and castration-resistant prostate cancers. $n = 3$ biological independent patients. Scale bars, $20\,\mu$m. **b**, Quantification of the number of CD11b$^+$CD15$^-$ cells in the tumour of castration-sensitive and castration-resistant prostate cancers (CSPC, $n = 51$; CRPC, $n = 51$ biological independent patients). Cells were counterstained with the nuclear marker DAPI (blue). Statistical analyses (negative binomial regression model): $P = 0.062$. **c**, MRIs of one representative sham-operated (Sham) or surgically castrated (CTX) $Pten^{PC-/-}$ mouse of the three analysed at different time points. **d**, Waterfall plot depicting proportional change in tumour response for sham ($n = 3$) and CTX ($n = 3$) $Pten^{PC-/-}$ mice. **e**, Prostate PMN-MDSC frequencies determined by flow cytometry in sham ($n = 3$) and CTX ($n = 3$) $Pten^{pc+/+}$ mice (12 weeks after castration). Statistical analyses (two-sided unpaired Student's t-test): $P = 0.85$. **f**, Schematic representation of the experiment.

Six-week-old C57BL/6 males were challenged subcutaneously with TRAMP-C1 cells. When tumours reached approximately $100\,\mathrm{mm}^3$, mice were sham-operated (sham, $n = 9$) or surgically castrated (CTX, $n = 5$). **g**, Tumour PMN-MDSC frequencies were determined by flow cytometry during castration-sensitive and castration-resistant phases. Sham CSPC, $n = 5$; CTX CSPC, $n = 4$; sham CRPC, $n = 8$; CTX CRPC $n = 6$. **h**, Schematic representation of the experiment. Six-week-old FVB males were challenged subcutaneously with MyC-CaP cells. When tumours reached approximately $100\,\mathrm{mm}^3$, mice were sham-operated (sham, $n = 3$) or surgically castrated (CTX, $n = 3$). **i**, Tumour PMN-MDSC frequencies were determined by flow cytometry during castration-sensitive and castration-resistant phases. Sham CSPC, $n = 3$; CTX CSPC, $n = 4$; sham CRPC, $n = 4$; CTX CRPC, $n = 3$. **b**, **d**, **e**, **g**, **i**, Data are mean $\pm$ s.e.m. **d**, **g**, **i**, Statistical analyses (unpaired two-sided Student's t-test): ns, not significant; *$P < 0.05$; **$P < 0.01$; ***$P < 0.001$. **f**, **h**, Statistical analyses (two-sided unpaired Student's t-test followed by Wilcoxon signed-rank test): *$P < 0.05$.
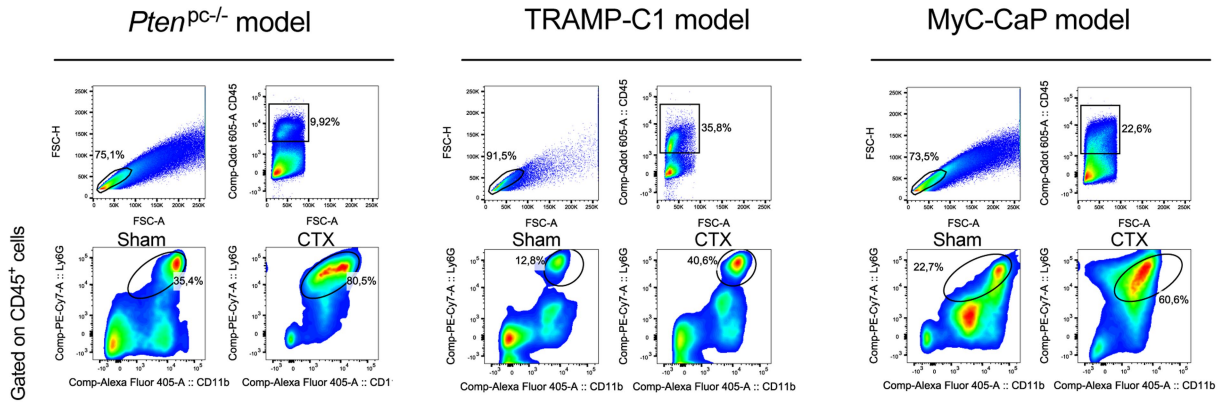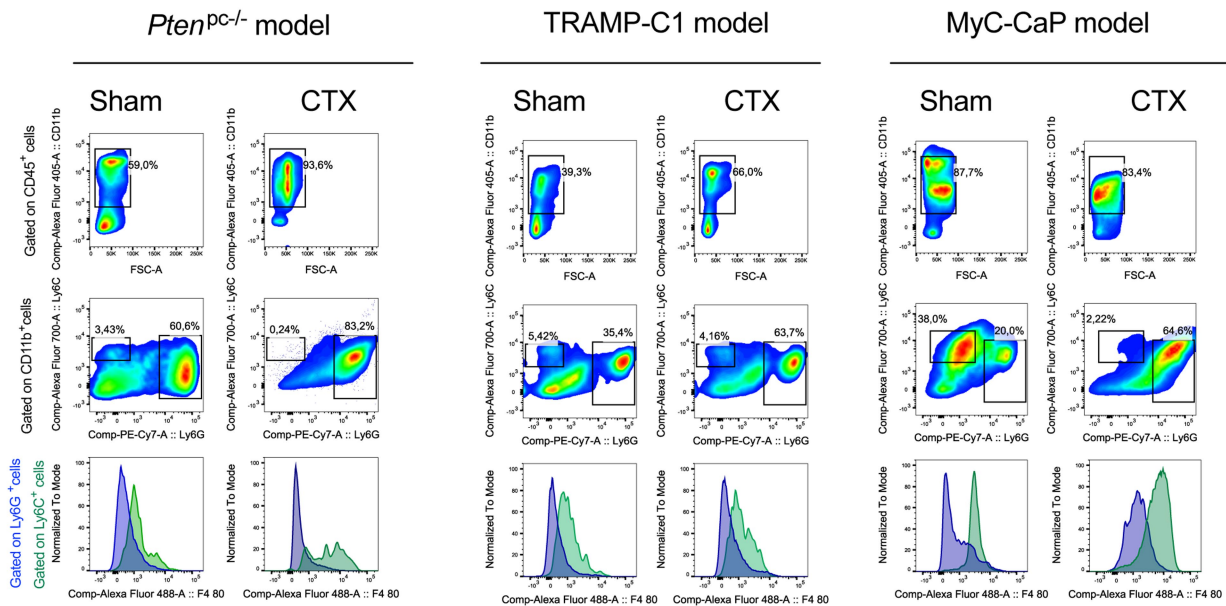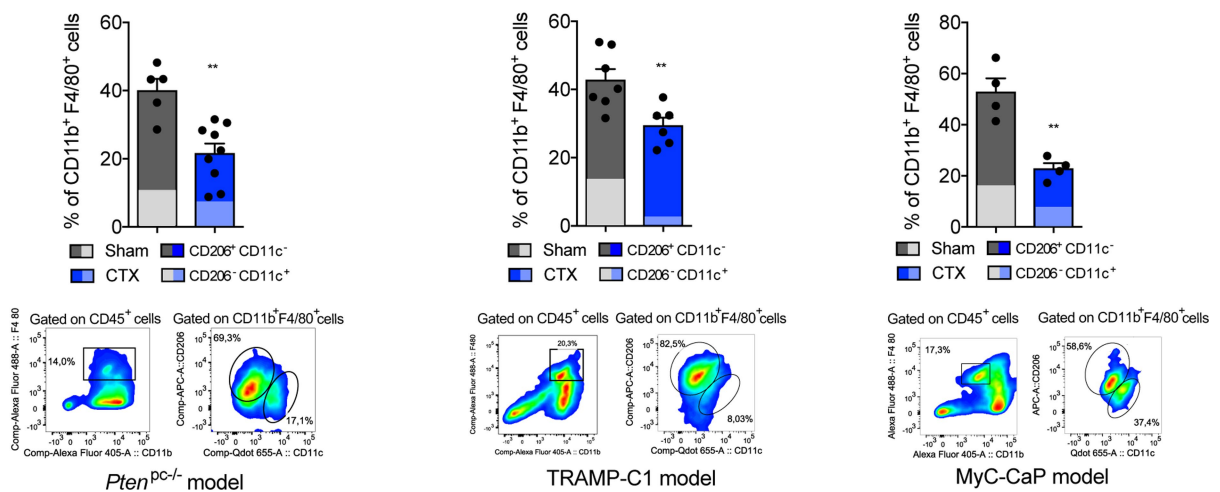
**Extended Data Fig. 2 | Multiparametric flow cytometry analysis of myeloid populations in the tumours of different CRPC mouse models.** **a**, Gating strategy relative to the quantification of PMN-MDSCs in the tumour of sham- and CTX-operated mice for $Pten^{PC-/-}$, TRAMP-C1 and MyC-CaP models. **b**, Representative dot plot reporting the Ly6G^{+} and Ly6C^{+} cells in the tumour of sham- and CTX-operated mice for $Pten^{PC-/-}$, TRAMP-C1 and MyC-CaP models. Data were validated in at

least three biological independent mice. **c**, Representative dot plot and quantification of CD11b^{+}F4/80^{+} cells and CD11c^{+}CD206^{−} (M1-like) or CD11c^{−}CD206^{+} (M2-like) macrophages in the tumour of sham- and CTX-operated mice for $Pten^{PC-/-}$ (sham, $n = 5$; CTX, $n = 9$), TRAMP-C1 (sham, $n = 7$; CTX, $n = 6$) and MyC-CaP (sham, $n = 4$; CTX, $n = 4$) models. Data are mean ± s.e.m. Statistical analyses (unpaired two-sided Student's t-test): **$P < 0.01$.
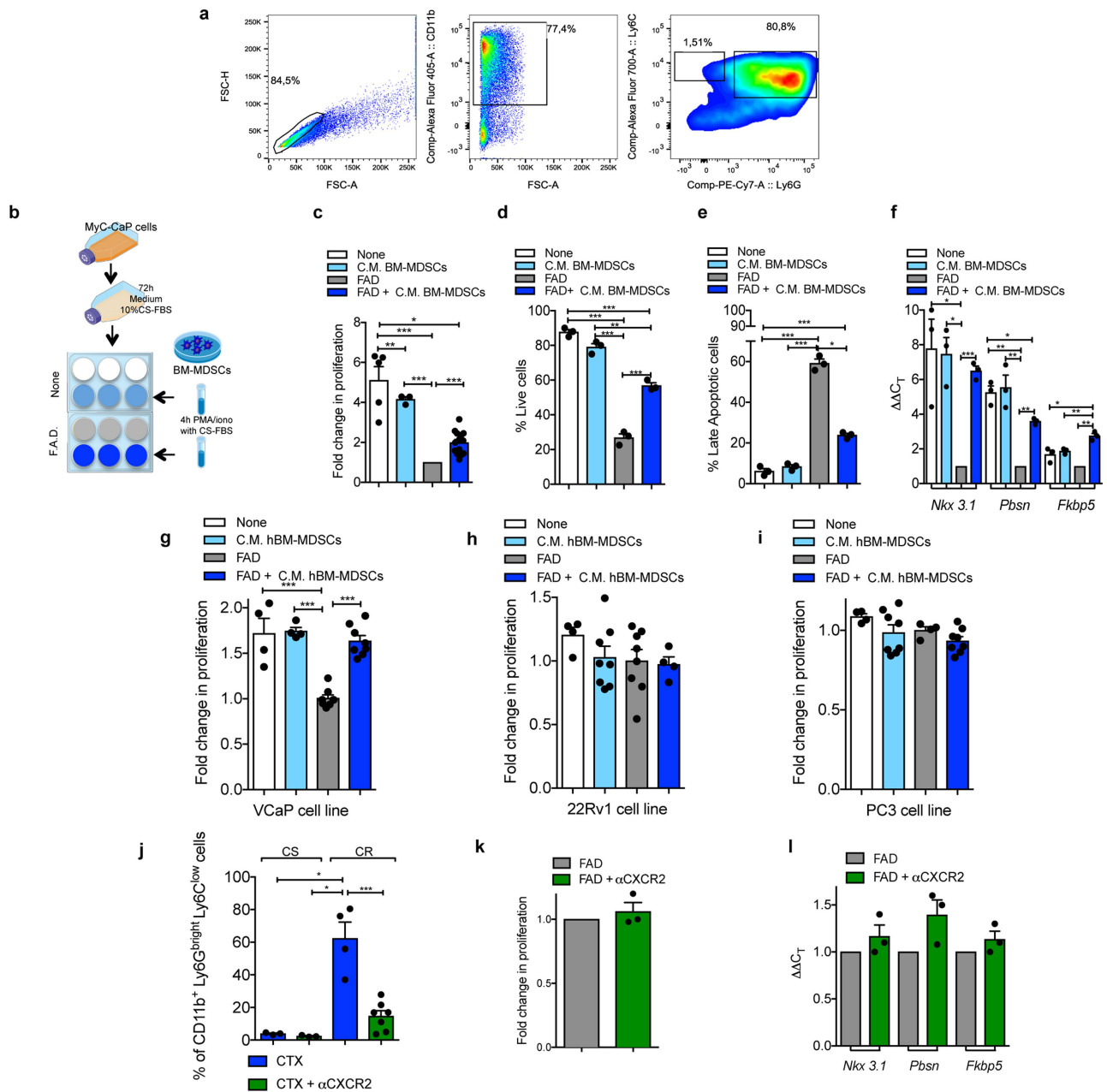
Extended Data Fig. 3 | Factors secreted by MDSCs promote insensitivity to ADT in androgen-dependent mouse and human prostate cancer cell lines and the CXCR2 antagonist impairs tumour recruitment of MDSCs in $Pten^{PC-/-}$ mice. a, Representative dot plot reporting the BM-MDSCs after in vitro differentiation. Data were validated in two biological independent experiments. **b**, Experimental scheme. **c**, Cell proliferation of MyC-CaP cells (none, $n = 5$; conditioned medium (C.M.) from BM-MDSCs, $n = 3$; FAD, $n = 13$; FAD and BM-MDSCs, $n = 13$ biological independent samples). **d**, Percentage of annexin V^- and 7AAD$^-$ MyC-CaP cells. **e**, Percentage of annexin V^+ and 7AAD$^+$ MyC-CaP cells. **f**, qRT–PCR analyses of the indicated genes in MyC-CaP cells. **g**, **h**, **i**, Cell proliferation of VCaP (none, $n = 4$; conditioned medium from human BM-MDSCs, $n = 4$; FAD, $n = 7$; FAD and human BM-MDSCs, $n = 8$ biological independent samples), 22Rv1 (none, $n = 4$; conditioned medium from human BM-MDSCs, $n = 8$; FAD, $n = 8$; FAD and human BM-MDSCs, $n = 4$ biological independent samples) and PC3 (none, $n = 4$; conditioned medium from human BM-MDSCs, $n = 8$; FAD, $n = 4$; FAD

and human BM-MDSCs, $n = 8$ biological independent samples) prostate cancer cells. **j**, Tumour MDSC frequencies determined by flow cytometry of prostate tumours of CTX $Pten^{PC-/-}$ mice treated or not with CXCR2 antagonist (αCXCR2) at completion of the study (12 weeks after CTX). CTX castration-sensitive, $n = 3$; CTX and CXCR2 antagonist castration-sensitive, $n = 3$; CTX castration-resistant, $n = 4$; CTX and CXCR2 antagonist castration-resistant, $n = 7$ biological independent mice. **k**, Cell proliferation of TRAMP-C1 cells after 72 h of treatment with CXCR2 antagonist. **l**, qRT–PCR analyses of the indicated genes in TRAMP-C1 cells after 24 h of treatment (fold change compared to the FAD condition). **k**, **l**, Aggregated data from three independent experiments are reported, fold change compared to the FAD condition. **c**–**l**, Data are mean ± s.e.m. **c**–**f**, $n = 3$ biological independent samples. **d**, **e**, **g**–**j**, Statistical analyses (unpaired two-sided Student's *t*-test): ns, not significant; *P < 0.05; **P < 0.01; ***P < 0.001. **c**, **f**, Statistical analyses (two-sided unpaired Student's *t*-test followed by Wilcoxon signed-rank test): *P < 0.05.
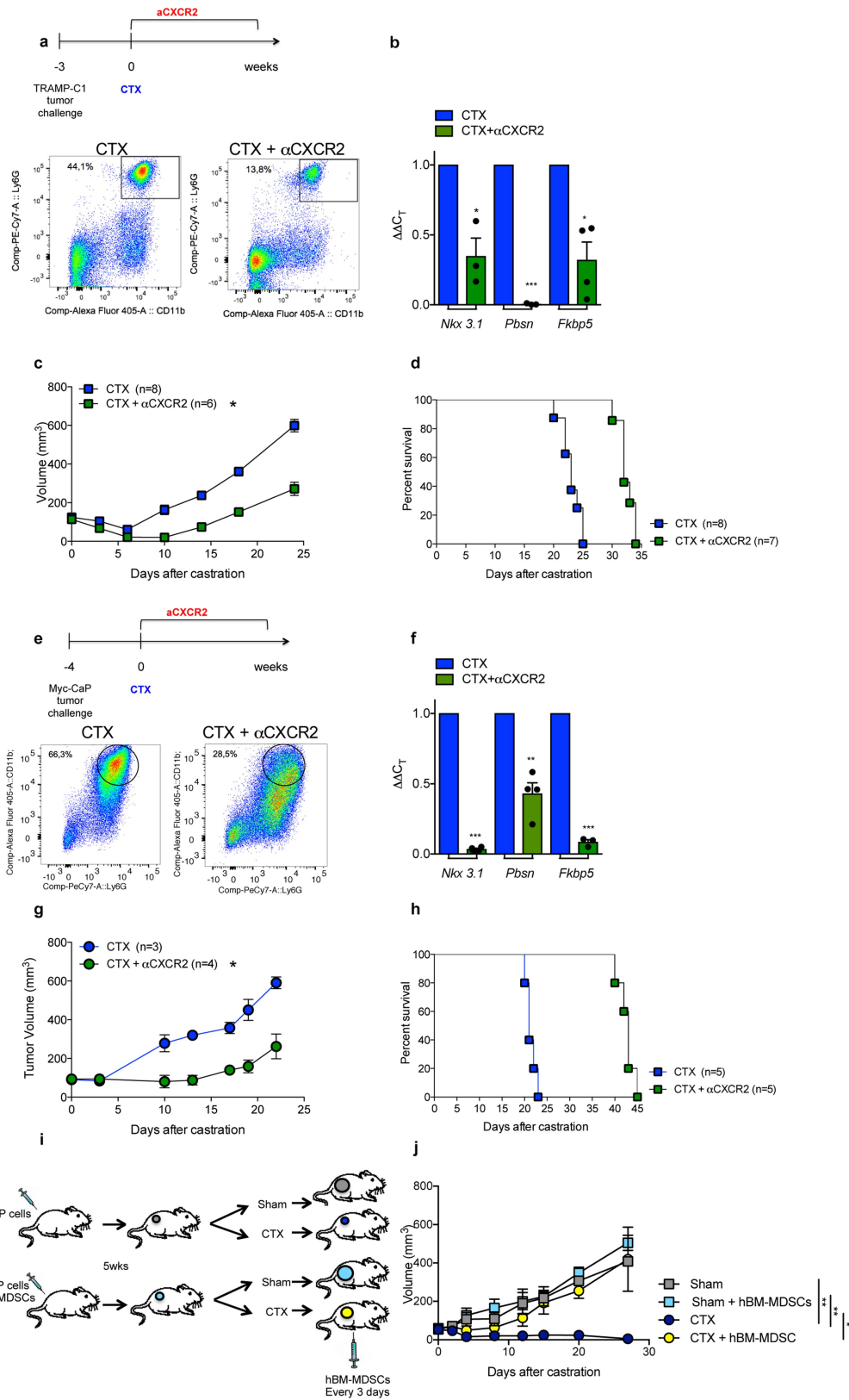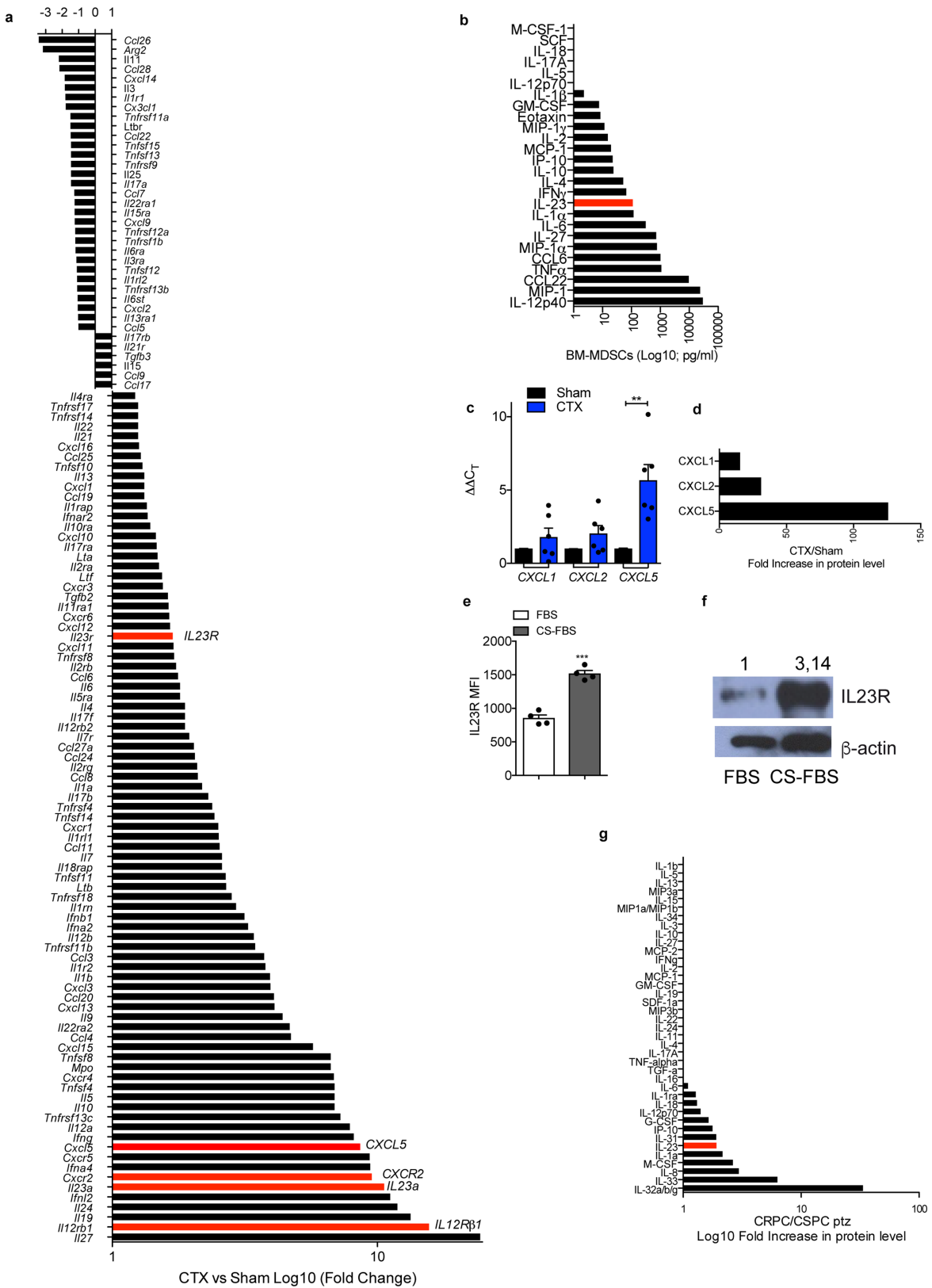
Extended Data Fig. 4 | See next page for caption.

Extended Data Fig. 4 | Impaired tumour recruitment of MDSCs enhances response to surgical castration in different allograft models of prostate cancers. a, Schematic representation of the experiment. Six-week-old C57BL/6 males were challenged subcutaneously with TRAMP-C1 cells. When tumours reached approximately 100 mm³, mice were surgically castrated and left untreated (CTX, $n = 8$) or treated with CXCR2 antagonist (CTX and CXCR2 antagonist, $n = 9$). Representative flow cytometry plots of PMN-MDSCs (CD11b⁺Ly6G⁺ cells, gated on CD45⁺ cells) in tumours for each experimental condition. **b**, qRT–PCR analyses of the indicated genes in the prostate tumours after CTX or CTX and CXCR2 antagonist treatment ($n = 3$ per group). Data are mean ± sem. Statistical analyses (unpaired two-sided Student's t-test): *$P < 0.05$; ***$P < 0.001$. **c**, Mean tumour volume (±s.e.m.) for each experimental group. Statistical analyses (unpaired two-sided Student's t-test followed by Wilcoxon signed-rank test): ***$P < 0.001$. **d**, Survival curves are reported in Kaplan–Meier plot. Statistical analyses (two-sided log-rank test): ***$P < 0.001$. **e**, Schematic representation of the experiment. Six-week-old FVB males were challenged subcutaneously with MyC-CaP cells. When tumours reached approximately 100 mm³, mice were surgically castrated and left untreated (CTX, $n = 5$) or treated with CXCR2 antagonist (CTX and CXCR2 antagonist, $n = 5$). Representative flow cytometry plots of PMN-MDSCs (CD11b⁺Ly6G⁺ cells, gated on CD45⁺ cells) in tumours for each experimental condition. **f**, qRT–PCR analyses of the indicated genes in the prostate tumours after CTX or CTX and CXCR2 antagonist treatment ($n = 3$ per group). Data are mean ± s.e.m. Statistical analyses (unpaired two-sided Student's t-test): **$P < 0.01$; ***$P < 0.001$. **g**, Average tumour volume (±s.e.m.) for each experimental group. Statistical analyses (two-sided unpaired Student's t-test followed by Wilcoxon signed-rank test): *$P < 0.05$. **h**, Survival curves reported as Kaplan–Meier plot. Statistical analyses (two-sided log-rank test): **$P < 0.01$. **i**, Schematic representation of the experiment. Six-week-old NOD/SCID males were challenged subcutaneously with LNCaP cells or with LNCaP cells and human BM-MDSCs. When tumours reached approximately 70 mm³, mice were sham-operated (sham, $n = 5$) or sham-operated and injected every three days intraperitoneally with 3×10^6 human BM-MDSCs (sham and human BM-MDSCs, $n = 5$) or surgically castrated and left untreated (CTX, $n = 8$) or treated with human BM-MDSCs (CTX and human BM-MDSCs, $n = 5$). **j**, Average tumour volume (±s.e.m.) for each experimental group. Statistical analyses (unpaired two-sided Student's t-test followed by Wilcoxon signed-rank test): **$P < 0.01$.

Extended Data Fig. 5 | See next page for caption.

Extended Data Fig. 5 | IL-23 pathway is the most upregulated in the tumour after castration. a, Gene expression of selected genes determined by NanoString nCounter gene expression assay in sham $Pten^{PC-/-}$ and CTX $Pten^{PC-/-}$ tumours. Data are shown as pool of $n = 5$. **b**, Analyses of the conditioned medium of bone marrow-derived MDSCs tested for the indicated soluble molecules by Mouse CytokineMAP B version 1.0. The graph shows the concentration of the indicated soluble molecules as $\log_{10}$ of the concentration found in the conditioned medium of BM-MDSCs, the values were subtracted of the background (culture medium). Data are shown as pool of $n = 10$. **c**, qRT–PCR analyses of the indicated genes in sham ($n = 6$) and CTX ($n = 6$) $Pten^{PC-/-}$ tumours. Data are mean ± s.e.m. of biological independent animals. Statistical analyses (unpaired two-sided Student's t-test): *$P < 0.05$. **d**, Protein level of CXCL1, CXCL2 and CXCL5 in CTX $Pten^{PC-/-}$ tumours. Data are analysed as ratio between CTX (pool of three samples) and sham (pool of three samples) $Pten^{PC-/-}$ tumours and reported as fold increase in protein level. **e, f**, IL-23R protein level analysed by flow cytometry and western blot on TRAMP-C1 cells under normal culture conditions (FBS) or androgen-deprivation culture conditions (charcoal-stripped FBS). $n = 4$ biological independent samples per group. **f**, Numbers indicate fold change in protein level. Loading control: anti-β-actin antibody. The western blot was validated at least twice. **g**, Protein profile of the plasma of patients with CSPC and CRPC. Data are analysed as ratio between CRPC (pool of 18 samples) and CSPC (pool of 17 samples) and reported as fold increase in protein level.
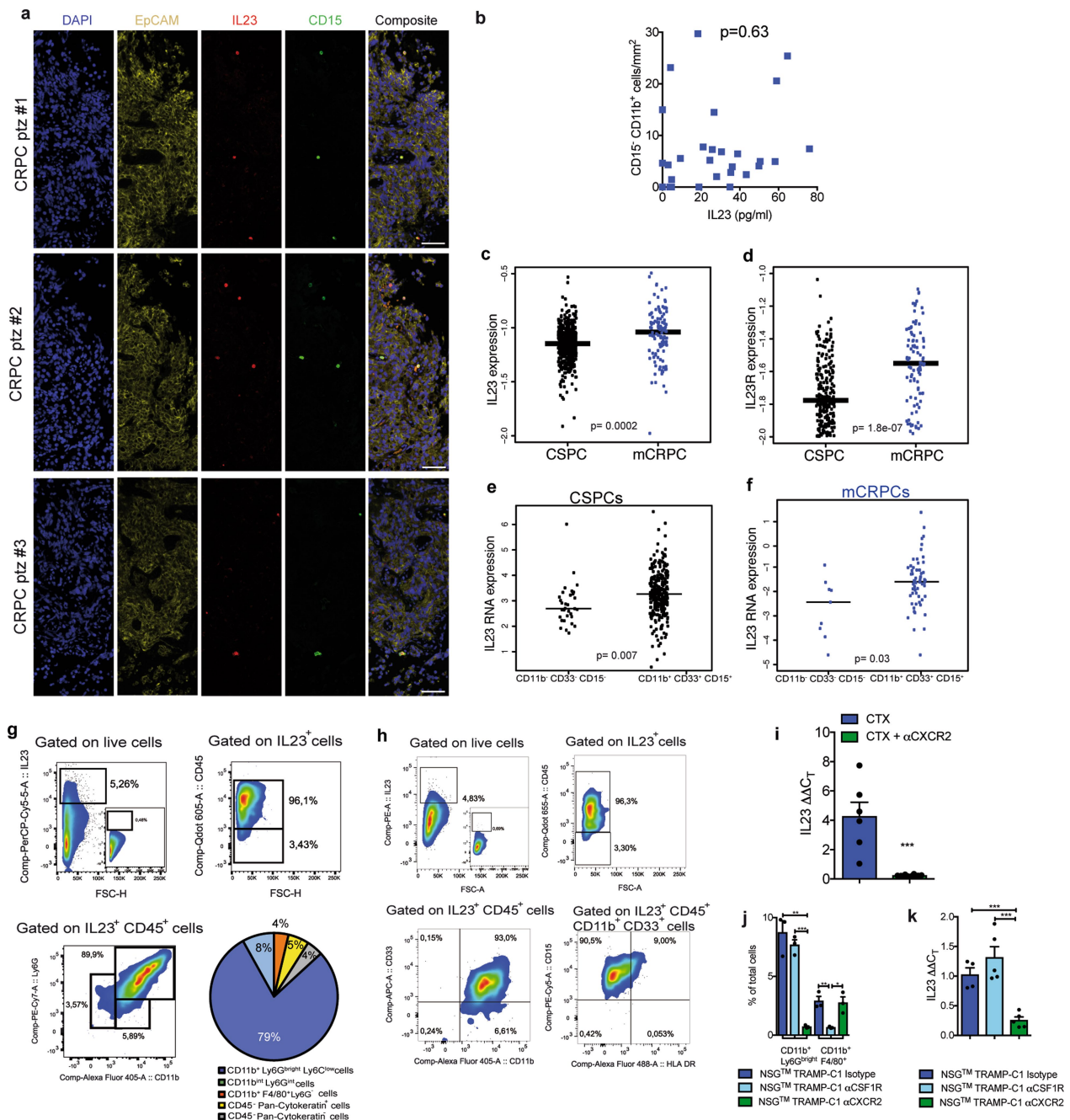
Extended Data Fig. 6 | Characterization of IL-23+ cells in the tumour of CTX $Pten^{PC-/-}$ mice and patients with CRPC. a, Multispectral microscopy images (EpCAM, yellow; CD15, green; IL-23, red) of three patients with CRPC. b, Correlation analyses of the numbers of CD15−CD11b+ cells in the tumour and IL-23 levels in the plasma of patients of CRPC ($n = 28$). Statistical analyses (negative binomial regression model): $P = 0.63$. c, d, IL23A and IL23R mRNA expression in the tumour of CSPCs ($n = 549$) and mCRPCs ($n = 116$). e, f, Expression of IL-23 in PMN-MDSC marker-positive (CD11b+CD33+CD15+) tumours from patients with CSPC or mCRPC. c–f, Statistical analyses (unpaired two-sided Student's t-test) are reported. g, Representative plots of IL-23+, CD45+ and CD45−, Ly6G^bright^CD11b+ and Ly6G^int^CD11b^int^, CD11b+F4/80+ cells pregated on the reported population in the tumour of CTX $Pten^{PC-/-}$ mice. IL-23 gate was decided based on isotype control

panel (insert). Pie chart shows the percentage of the different subsets gated on IL-23+ cells in the tumour of $Pten^{PC-/-}$ mice (mean, $n = 9$). h, qRT–PCR analyses of IL-23 in the prostate tumours of castrated (CTX; $n = 6$) or castrated and treated with CXCR2 antagonist (CTX + CXCR2 antagonist; $n = 7$) $Pten^{PC-/-}$ mice. Data are mean ± s.e.m. i, PMN-MDSC and TAM frequencies determined by flow cytometry in the tumour of castrated NSG TRAMP-C1 allografts upon treatment with isotype, CSF1R antibody, CXCR2 antagonist. Data are mean ± s.e.m. ($n = 3$ per group). j, qRT–PCR analyses of IL-23 in the tumour of castrated NSG TRAMP-C1 allografts upon treatment with isotype ($n = 4$), CSF1R antibody ($n = 5$), CXCR2 antagonist ($n = 5$). Data are mean ± s.e.m. Each dot represents a biological independent animal. h–j, Statistical analyses (unpaired two-sided Student's t-test): *$P < 0.05$; **$P < 0.01$; ***$P < 0.01$.

a

b
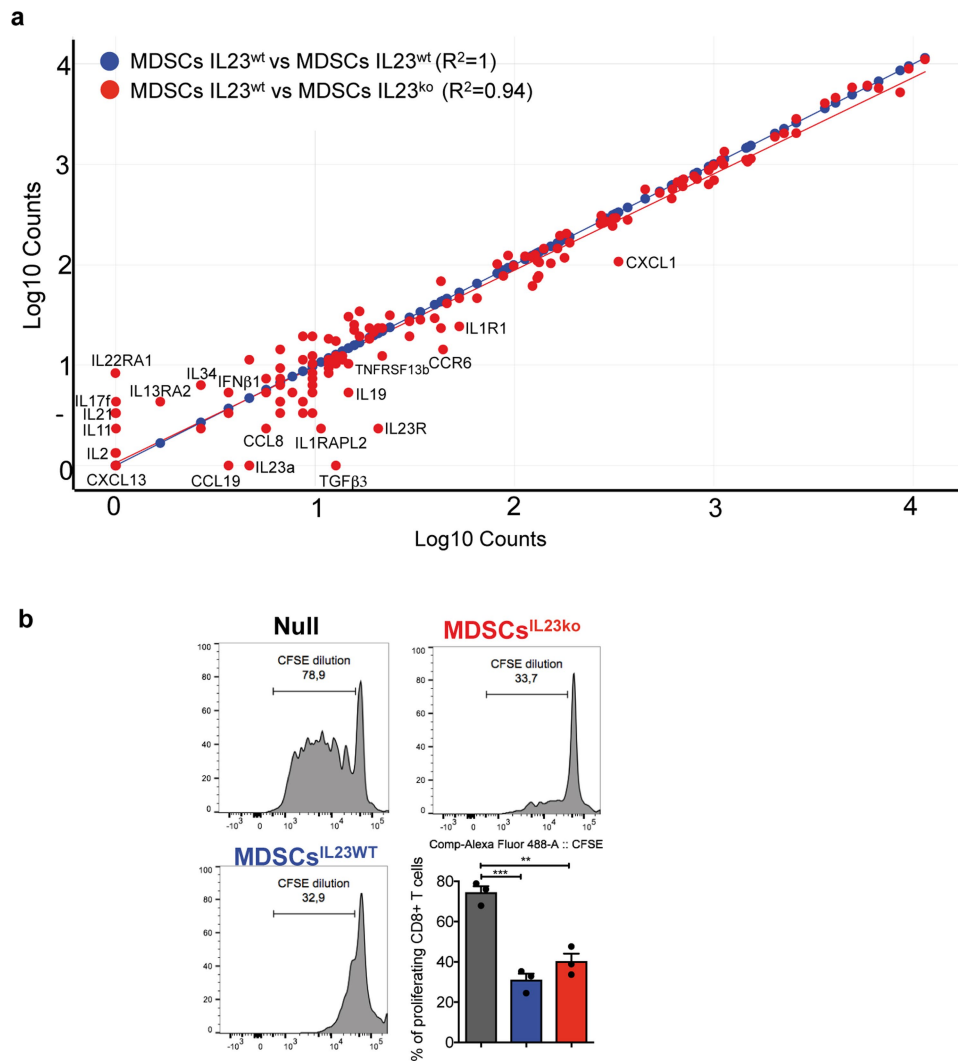
**Extended Data Fig. 7 | $Il23a^{WT}$ and $Il23a^{KO}$ BM-MDSCs have equal secretome and equal immunosuppressive capability. a**, Correlation analyses of the gene expression of selected genes determined by NanoString nCounter gene expression assay in $Il23a^{WT}$ and $Il23a^{KO}$ BM-MDSCs shown as scatter plot analyses. Data are shown as pool of $n = 10$. R^2 values were determined using linear regression analyses.

b, Representative flow cytometry plots of CFSE dilution (gated on CD8^{+} cells) and quantification of proliferating CD8^{+} T cells exposed to conditioned medium from $Il23a^{WT}$ and $Il23a^{KO}$ BM-MDSCs. Data are mean ± s.e.m. of three independent biological samples. Statistical analyses (unpaired two-sided Student's t-test): **$P < 0.01$; ***$P < 0.01$.
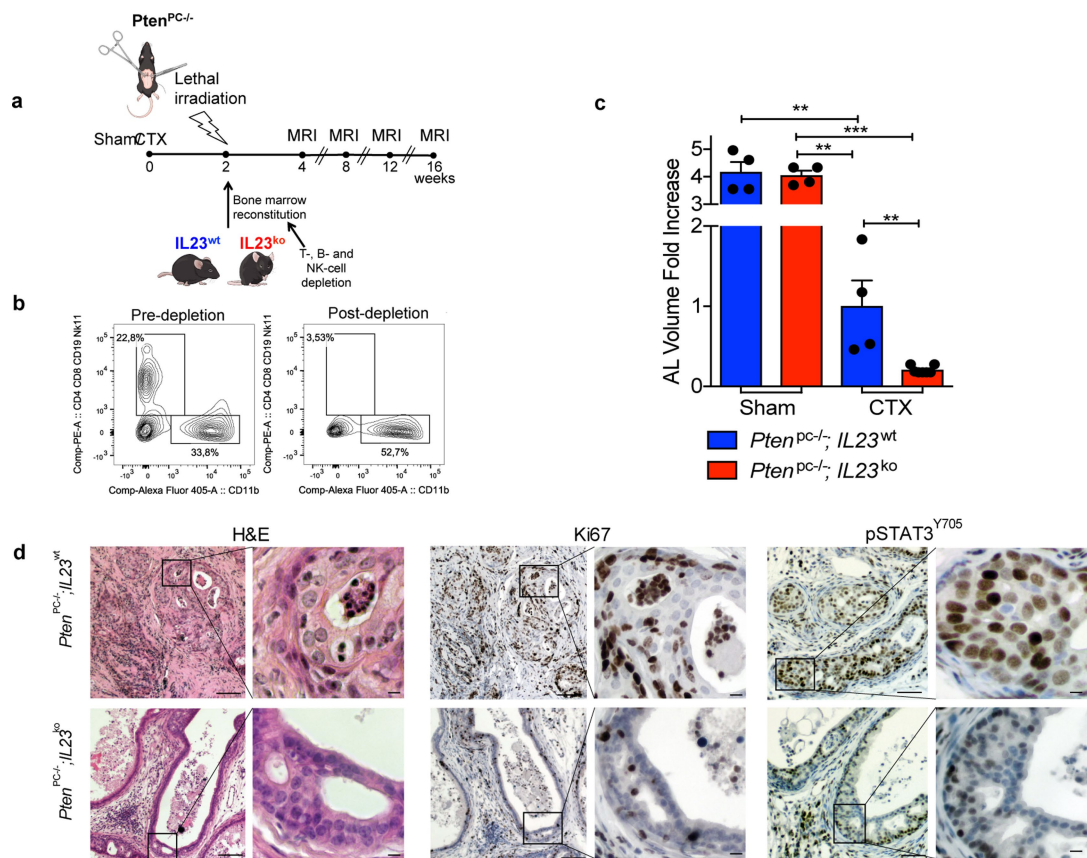
Extended Data Fig. 8 | Genetic inhibition of IL-23 limits resistance to castration in prostate cancer in $Pten^{PC-/-}$ mice. a, Experimental set-up. Sham-operated (sham) or castrated (CTX) $Pten^{PC-/-}$ mice were lethally irradiated and transplanted with bone marrow precursors depleted of T, B and NK cells from $Il23a^{WT}$ and $Il23a^{KO}$ mice. The mice were then monitored by MRI for tumour progression. **b**, Representative dot plot of bone marrow precursors pre- and post-depletion of T, B, and NK cells. Data were validated in two biological independent experiments. **c**, Quantification of the tumour size of sham-operated $Pten^{PC-/-}Il23a^{WT}$ ($n=4$) and $Pten^{PC-/-}Il23a^{KO}$ ($n=4$), and castrated $Pten^{PC-/-}Il23a^{WT}$

($n=4$) and $Pten^{PC-/-}Il23a^{KO}$ ($n=7$) mice at the completion of the study is reported as fold increase of the prostate anterior lobe (AL) volume (fold change compared to the CTX $Pten^{PC-/-}Il23a^{WT}$ group). Data are mean ± s.e.m. Statistical analyses (unpaired two-sided Student's t-test): **$P < 0.01$, ***$P < 0.001$. **d**, Haematoxylin and eosin, Ki-67 and pSTAT3(Y705) immunohistochemical staining (Ki-67 and pSTAT3(Y705), brown; nuclei, blue) of one representative $Pten^{PC-/-}Il23a^{WT}$ and $Pten^{PC-/-}Il23a^{KO}$ mouse of at least three mice analysed at completion of the study. Scale bars, $50\,\mu m$ (left) and $25\,\mu m$ (right).
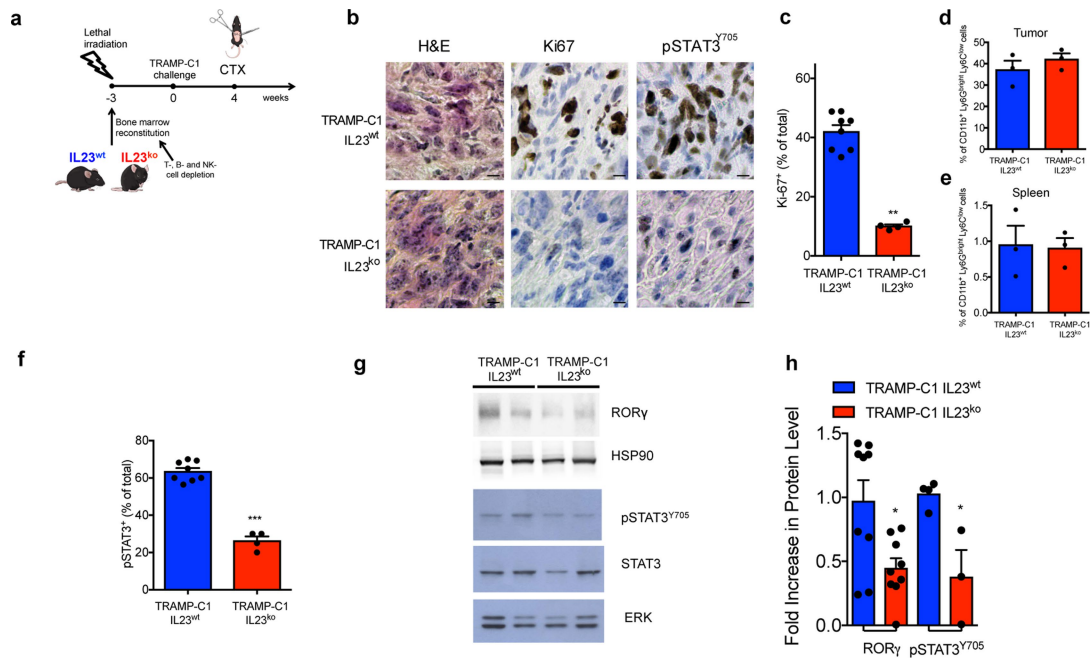
Extended Data Fig. 9 | Genetic inhibition of IL-23 limits resistance to castration in prostate cancer in TRAMP-C1 allograft model in vivo.
a, Schematic representation of the experiment. Six-week-old C57BL/6 males were lethally irradiated and transplanted with bone marrow precursors from $Il23a^{WT}$ and $Il23a^{KO}$ mice. After the bone marrow engraftment, the animals were challenged subcutaneously with TRAMP-C1 cells. When tumours reached approximately 100 mm^3, mice were surgically castrated and monitored for tumour progression. **b**, Haematoxylin and eosin, Ki-67 and pSTAT3(Y705) immunohistochemical staining (Ki-67 and pSTAT3(Y705), brown; nuclei, blue) of representative TRAMP-C1 $Il23a^{WT}$ and TRAMP-C1 $Il23a^{KO}$ mice. Scale bars, 25 μm. **c**, Quantification of Ki-67$^+$ cells is reported as a percentage of the total number of cells. TRAMP-C1 $Il23a^{WT}$ ($n = 8$) and TRAMP-C1 $Il23a^{KO}$ ($n = 4$), one tumour per mouse, mean of three sections per tumour, $\geq$3 fields per section. Data are mean $\pm$ s.e.m. of biologically independent mice. Statistical analyses (unpaired two-sided Student's t-test): **$P < 0.01$. **d**, **e**, PMN-MDSC

frequencies determined by flow cytometry in the tumour and in the spleen of TRAMP-C1 $Il23a^{WT}$ ($n = 3$) and TRAMP-C1 $Il23a^{KO}$ ($n = 3$) mice 10 days after castration. Data are mean $\pm$ s.e.m. **f**, Quantification of pSTAT3(Y705) reported as a percentage of the total number of cells. TRAMP-C1 $Il23a^{WT}$ ($n = 8$) and TRAMP-C1 $Il23a^{KO}$ ($n = 4$), one tumour per mouse, mean of three sections per tumour, $\geq$3 fields per section. Statistical analyses (unpaired two-sided Student's t-test): ***$P < 0.001$. **g**, Western blot for RORγ, pSTAT3(Y705) and total STAT3 levels in prostate tumours of TRAMP-C1 $Il23a^{WT}$ and TRAMP-C1 $Il23a^{KO}$ mice. Loading control: HSP90 antibody or total ERK antibody. The western blot was validated at least twice. **h**, Quantification is reported as mean $\pm$ s.e.m. of biological independent experiments: TRAMP-C1 $Il23a^{WT}$ RORγ, $n = 9$; and TRAMP-C1 $Il23a^{KO}$ RORγ, $n = 9$; TRAMP-C1 $Il23a^{WT}$ pSTAT3(Y705), $n = 4$; and TRAMP-C1 $Il23a^{KO}$ pSTAT3(Y705), $n = 3$. Statistical analyses (unpaired two-sided Student's t-test): *$P < 0.05$.
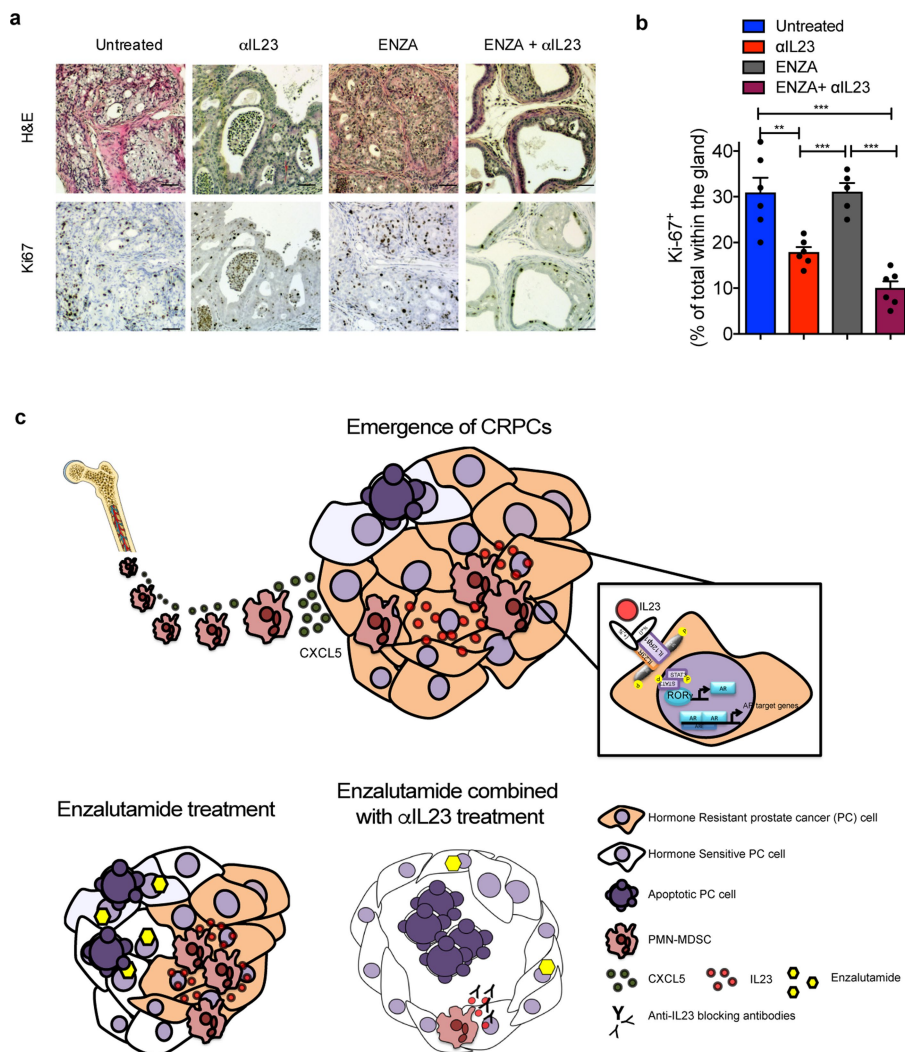
Extended Data Fig. 10 | Pharmacological inhibition of IL-23 in association with ADT delays disease progression in prostate cancer.
a, Haematoxylin and eosin and Ki-67 immunohistochemical staining (Ki-67, brown; nuclei, blue) of representative castrated $Pten^{PC-/-}$ mice treated with IL-23, ENZA or both. Scale bars, 50 μm. **b**, Quantification of Ki-67 reported as a percentage of total within the glands. One tumour per mouse, three sections per tumour, ≥3 fields per section. Data are mean ± s.e.m. of biologically independent animals. Untreated, $n = 6$; IL-23, $n = 6$; ENZA, $n = 5$ or both, $n = 6$. Statistical analyses (unpaired two-sided Student's t-test): **$P < 0.01$; ***$P < 0.001$. **c**, After castration,

PMN-MDSCs progressively infiltrate the tumour bed mainly recruited by CXCL5. Within the tumour, PMN-MDSCs start to produce higher amount of IL-23, thus establishing a positive-feedback loop that induces the overexpression of IL-23R on the tumour epithelial cells and confer resistance to castration in prostate cancer by activating the STAT3–RORγ pathway. ENZA treatment can block the AR, inducing sensitiveness of prostate cancer cells to androgen deprivation, but the persistent presence of PMN-MDSC-derived IL-23 rescues the drug sensitiveness leading to ADT resistance. Anti-IL-23 treatment reinstates sensitivity to castration in prostate cancer enhancing the efficacy of ENZA.

nature research

Corresponding author(s):   Andrea Alimonti

Reporting Summary

Nature Research wishes to improve the reproducibility of the work that we publish. This form provides structure for consistency and transparency in reporting. For further information on Nature Research policies, see Authors & Referees and the Editorial Policy Checklist.

Statistical parameters

When statistical analyses are reported, confirm that the following items are present in the relevant location (e.g. figure legend, table legend, main text, or Methods section).

n/a	Confirmed	
☐	☒	The exact sample size (*n*) for each experimental group/condition, given as a discrete number and unit of measurement
☐	☒	An indication of whether measurements were taken from distinct samples or whether the same sample was measured repeatedly
☐	☒	The statistical test(s) used AND whether they are one- or two-sided *Only common tests should be described solely by name; describe more complex techniques in the Methods section.*
☒	☐	A description of all covariates tested
☐	☒	A description of any assumptions or corrections, such as tests of normality and adjustment for multiple comparisons
☐	☒	A full description of the statistics including central tendency (e.g. means) or other basic estimates (e.g. regression coefficient) AND variation (e.g. standard deviation) or associated estimates of uncertainty (e.g. confidence intervals)
☐	☒	For null hypothesis testing, the test statistic (e.g. *F*, *t*, *r*) with confidence intervals, effect sizes, degrees of freedom and *P* value noted *Give P values as exact values whenever suitable.*
☒	☐	For Bayesian analysis, information on the choice of priors and Markov chain Monte Carlo settings
☒	☐	For hierarchical and complex designs, identification of the appropriate level for tests and full reporting of outcomes
☒	☐	Estimates of effect sizes (e.g. Cohen's *d*, Pearson's *r*), indicating how they were calculated
☐	☒	Clearly defined error bars *State explicitly what error bars represent (e.g. SD, SE, CI)*

Our web collection on statistics for biologists may be useful.

Software and code

Policy information about availability of computer code

Data collection	nCounter analysis system (NanoString Technologies, Seattle, WA); BD Fortessa (DB Bioscience); Vectra (Perkin Elmer) system.
Data analysis	inForm v2.1.1 software (PerkinElmer), GraphPad Prism version 7, FlowJo software v10.1 (TreeStar, Ashland, OR), Image J software, Repertoire Genesis Inc. software, STAR (v2.5.2b)

For manuscripts utilizing custom algorithms or software that are central to the research but not yet described in published literature, software must be made available to editors/reviewers upon request. We strongly encourage code deposition in a community repository (e.g. GitHub). See the Nature Research guidelines for submitting code & software for further information.

Data

Policy information about availability of data

All manuscripts must include a data availability statement. This statement should provide the following information, where applicable:
- Accession codes, unique identifiers, or web links for publicly available datasets
- A list of figures that have associated raw data
- A description of any restrictions on data availability

Source Data (Graph) for the main figures and all the experiments involving animals of the Extended data figures are provided. Source Data (gels) for all the WB reported in the paper are provided. All the other results can be available from the corresponding authors upon reasonable request.

Field-specific reporting

Please select the best fit for your research. If you are not sure, read the appropriate sections before making your selection.

☒ Life sciences   ☐ Behavioural & social sciences   ☐ Ecological, evolutionary & environmental sciences

For a reference copy of the document with all sections, see nature.com/authors/policies/ReportingSummary-flat.pdf

Life sciences study design

All studies must disclose on these points even when the disclosure is negative.

Sample size	Sample size was chosen taking in consideration the means of the target values between the experimental group and the control group, the standard error and the statistical analysis used. For animal studies, sample size was defined on the basis of past experience with the models12, to detect differences of 20% or greater between the groups (10% significance level and 80% power). For ethical reasons, the minimum number of animals necessary to achieve the scientific objectives was used.
Data exclusions	Grubb's test was applied to exclude outliers.
Replication	For each experiments the number of biological independent animal/sample/patient is reported in the figure legend. Gene expression by NanoString nCounter gene expression assay, mouse CytokineMAP B version 1.0, and protein profile using Human XL Cytokine Array Kit or Mouse XL Cytokine Array Kit was performed once and then validated with other methods with biological independent animals/patients.
Randomization	Animals were allocated randomly to each treatment group. Different treatment groups were processed identically, and animals in different treatment groups were exposed to the same environment.
Blinding	In IHC analyses, the investigators were unaware of the experimental groups.

Reporting for specific materials, systems and methods

Materials & experimental systems

n/a	Involved in the study
☒	☐ Unique biological materials
☐	☒ Antibodies
☐	☒ Eukaryotic cell lines
☒	☐ Palaeontology
☐	☒ Animals and other organisms
☐	☒ Human research participants

Methods

n/a	Involved in the study
☒	☐ ChIP-seq
☐	☒ Flow cytometry
☐	☒ MRI-based neuroimaging

Antibodies

Antibodies used	-Immune tumor microenvironment characterization After neutralization of unspecific binding with αCD16/CD32 (clone 93), single-cell suspensions were stained with specific mAb (primary antibodies directly conjugated) to assess the phenotype and diluted 1:200. The antibodies used were: αCD45 (clone 30-F11, Lot. B235438); αLy-6G (clone 1A8, Lot B194432); αLy6C (clone HK1.4, Lot. B243043), αCD11b (clone M1/70, Lot. B233927); αF4/80 (clone BM8, Lot. 4305911), αCD206 (clone C068C2, Lot. B230155), αCD11c (clone N418, Lot. B226270), αB220 (clone RA3-6B2, Lot. B210434), αCD3 (clone 145-2C11, Lot. B241616), αCD8 (clone 53-6.7, Lot. B193838), αCD4 (clone GK1.5, Lot. B240053), αNK1.1 (clone PK136, Lot. 4291566), αCD90.2 (clone 30-H12, Lot. B190542), αPDL1 (clone 10F.9G2, Lot. B191993), αEpCAM (clone G8.8, Lot. B230070), αPan-Cytokeratin (clone C11, Lot. 4528S), αIL17 (clone TC11-18H10.1, Lot. B201753), αIL23p19 (clone FC23CPG, Lot. 4321359), Isotype (Rat/IgG1,kappa, eBRG1) αIL23R (clone 12B2B64, Lot. 4321359), For flow gating we used isotype controls of florescence minus one controls. All the antibodies were purchased from eBioscience or Biolegend. -Murine Immunohistochemistry and Immunofluorescence: Sections were stained for anti-Ki67 (Clone SP6; Lab Vision Corporation), anti-pSTAT3 (TYR705; clone D3A7; Cell Signaling). DAPI (#70238421, Roche), anti-IL23 (ab45420; Abcam), anti-Ly6G (RB6-8C5; GeneTex). -Immune tumor microenvironment characterization in prostate cancer patients: Single-cell suspensions were stained with specific mAb (primary antibodies directly conjugated) and diluted 1:200 to assess the phenotype. The antibodies used were: αCD45RA (clone MEM-56, 1:50); αCD33 (clone WM53); αCD11b (clone ICRF44); αCD15 (clone W6D3), αHLA-DR (clone L243), αIL23p19 (clone 23DCDP). - Multiplex IF in formalin fixed paraffin embedded tissue section: Multiplex immunofluorescence: CD15 (#M3631, Dako, clone Carb-3), CD33 (#ab11032, Abcam, clone 6C5/2), CD11b (#ab52477,

Abcam, clone EP1345Y) and EpCAM Alexa Fluor® 647 conjugate (#5447S, CellSignaling, clone VU1D9) anti-CD15 (#M3631, Dako, clone Carb-3, dilution 1:200), rabbit monoclonal (IgG) antibody anti-IL23 (#ab190356, Abcam, clone EPR5585(N), dilution 1:100) and mouse monoclonal (IgG1) anti EpCAM antibody (#2929S, CellSignaling, clone VU1D9, dilution 1:500)
-Western blot analyses:rabbit polyclonal anti-HSP90 (1:1000 dilution, Cell Signaling), rabbit polyclonal anti-phospho-Stat3 (Tyr705) (1:1000 dilution, Cell Signaling), rat monoclonal anti-RORγt (5:1000 dilution, clone AFKJS-9, eBioscience), rabbit polyclonal anti-IL23R (H-300) (1:1000 dilution, Santa Cruz).

| Validation | IHC was performed on 4μm formalin-fixed paraffin embedded (FFPE) tissue sections using an automated staining platform (Bond-RX, Leica Microsystems). Optimal antibody concentrations were determined with primary antibodies against CD15 (#M3631, Dako, clone Carb-3, dilution 1:200), CD33 (#ab11032, Abcam, clone 6C5/2, dilution 1:100), CD11b (#ab52477, Abcam, clone EP1345Y, dilution 1:100) IL23 (#ab190356, Abcam, clone EPR5585 (N), dilution 1:100) and EpCAM (#2929S, CellSignaling, clone VU1D9, dilution 1:500). Antibody labelling was detected with the Bond Polymer Refine Detection Kit (#DS9800, Leica Microsystems). 3,3-diaminobenzidine tetrahydroxychloride (DAB) was used as chromogen and the slides were counterstained with hematoxylin. Human control included colorectal specimens. In each staining batch, positive and negative controls were incubated with and without primary antibody. |

Eukaryotic cell lines

Policy information about cell lines

Cell line source(s)	TRAMP-C1 cells line, MYC-CaP cell line, and LNCaP cell line, VCaP cell line, 22Rv1 cell line, PC3 cell line were received by ATCC. TRAMP-C1 IL23Rko cell line was generated in the lab with CRISPR-Cas9 methodology.
Authentication	TRAMP-C1 cells line, MYC-CaP cell line, and LNCaP cell line, VCaP cell line, 22Rv1 cell line, PC3 cell line were received by ATCC and no other authentication method was performed. TRAMP-C1 IL23Rko cell line was generated in the lab and authenticated by WB and FACS for the deletion of IL23R.
Mycoplasma contamination	All the cell lines were regularly tested for mycoplasma (MycoAlert Mycoplasma Detection kit).
Commonly misidentified lines (See ICLAC register)	No commonly misidentified cell lines were used.

Animals and other organisms

Policy information about studies involving animals; ARRIVE guidelines recommended for reporting animal research

Laboratory animals	All mice were maintained under specific pathogen-free conditions in the IRB facility and experiments were performed according to national guidelines and regulations. All the animal experiments have been approved by the local ethics committee (TI13/2015 and TI04/2017). Male C57BL/6, FVB, NSGTM, NOD SCID mice 6–8 weeks of age were purchased from Jackson Laboratories (Envigo) and acclimated for at least a week before use. Male C57BL/6 IL-23p19KO (IL23ko) mice27 were kindly provided by Prof. Federica Sallusto (IRB, Bellinzona) and used 8 weeks old. Male Ptenpc-/- mice were generated and genotyped as previously described17. Female PtenloxP/loxP mice were crossed with male PB-Cre4 transgenic mice and genotyped for Cre using following primers: primer 1 (5'-AAAAGTTCCCCTGCTGATGATTTGT-3') and primer 2 (5'-TGTTTTTGACCAATTAAAGTAGGCTGTG-3') for PTENloxP/loxP; primer1 (5' TGATGGACATGTTCAGGGATC 3') and primer2 (5'CAGCCACCAGCTTGCATGA 3') for Probasin-CRE. Surgical castration was performed under anesthesia with isoflurane. Male Ptenpc-/- mice were 9/10 weeks old at the time of castration. Mice were monitored postoperatively for recovery from anesthesia and checked daily for 4 days postoperatively. Surgical skin clips were removed on postoperative day 5. Mice undergoing treatment were administered control vehicle or therapeutic doses of the appropriate agents. Any mouse suffering distress or greater than 15% weight loss during treatment was euthanized by CO2 asphyxiation. At the completion of study, mice were euthanized by CO2 asphyxiation and tissue was collected for histology, mRNA analysis, protein analysis and single cell suspensions for flow cytometry. Animals were sacrificed when the tumor reached approximately 600 mm3. The local ethic committee allows performing in vivo experiments with maximal tumor size of 1000 mm3.
Wild animals	No wild animals were used in the study.
Field-collected samples	No field-collected samples were used.

Human research participants

Policy information about studies involving human research participants

| Population characteristics | All patient samples consenting to the trial were men with prostate cancer.
Fifty-one patients with CRPC being treated at The Royal Marsden NHS Foundation Trust Hospital with sufficient formalin fixed paraffin embedded matched CSPC and CRPC biopsies for multiplex IF were selected as reported below:
CSPC biopsy: Age at diagnosis 61.2 (+/-6) years. Staging: T2, T3, T4, NR, N0, N1, NR, M0, M1 and NR. Biopsy sites: Prostate core, prostatectomy, TURP, Lymph node. Gleason: N=34 with 8-10, N=13 with 7, N=2 <6, N=2 NS. Mean of PSA= 56 ug/L.
CRPC biopsy: Site of metastasis: BM trephine, Lymphonode, liver, TURP, soft tissue. Treatments: Docetaxel, Cabazitaxel, Abiraterone, enzalutamide. Consistent with this, plasma from 120 CRPC patients with sufficient samples stored (including 28 plasma samples within 40 days of CRPC biopsy) and 20 CSPC patients were analyzed for IL23 levels.
Four patients with CRPC, enrolled at Azienda Ospedaliera di Padova, and four patients with CSPC, enrolled at IRCCS Ospedale San Raffaele, were selected to perform the immune tumor microenvironment characterization by flow cytometry analyses. |

Recruitment	All patients given written informed consent and were enrolled in institutional protocols approved either by the Royal Marsden NHS Foundation Trust Hospital (London, UK) ethics review committee (reference no. 04/Q0801/60) or the IRCCS Ospedale San Raffaele (Milan, Italy) ethics review committee (reference no. 99/INT/2004; 58/INT/2010) or Azienda Ospedaliera di Padova (Padova, Italy) ethics review committee (reference no.CESC/958P/2005). Human biological samples were sourced ethically and their research use was in accord with the terms of the informed consent provided. Case selection was therefore independent and blinded to baseline characteristics, treatments received, clinical outcome and molecular characterization to reduce any potential self-selection bias.

Flow Cytometry

Plots

Confirm that:

☒ The axis labels state the marker and fluorochrome used (e.g. CD4-FITC).

☒ The axis scales are clearly visible. Include numbers along axes only for bottom left plot of group (a 'group' is an analysis of identical markers).

☒ All plots are contour plots with outliers or pseudocolor plots.

☒ A numerical value for number of cells or percentage (with statistics) is provided.

Methodology

Sample preparation	Tumors were disaggregated and digested in collagenase D and DNAse for 30 minutes at 37°C to obtain single-cell suspension. For intracellular cytokine detection cells where stimulated for 5 hours with PMA/ionomycin plus Golgi Plug. After neutralization of unspecific binding with αCD16/CD32 (clone 93), single-cell suspensions were stained with specific mAb (primary antibodies directly conjugated) to assess the phenotype. The antibodies used were: αCD45 (clone 30-F11); αLy-6G (clone 1A8); αLy6C (clone HK1.4), αCD11b (clone M1/70); αF4/80 (clone BM8), αCD206 (clone C068C2), αCD11c (clone N418), αB220 (clone RA3-6B2), αCD3 (clone 145-2C11), αCD8 (clone 53-6.7), αCD4 (clone GK1.5), αNK1.1 (clone PK136), αCD90.2 (clone 30-H12), αPDL1 (clone 10F.9G2), αEpCAM (clone G8.8), αPan-Cytokeratin (clone C11), αIL17 (clone TC11-18H10.1), αIL23p19 (clone FC23CPG), αIL23R (clone 12B2B64). For flow gating we used isotype controls of florescence minus one controls. All the antibodies were purchased from eBioscience or Biolegend. Immune tumor microenvironment characterization in prostate cancer patients Tumors were disaggregated and digested in collagenase I and DNAse for 20 minutes at 37°C to obtain single-cell suspension. For intracellular cytokine detection cells where stimulated for 5 hours with PMA/ionomycin plus Golgi Plug. Single-cell suspensions were stained with specific mAb (primary antibodies directly conjugated) to assess the phenotype. The antibodies used were: αCD45RA (clone MEM-56); αCD33 (clone WM53); αCD11b (clone ICRF44); αCD15 (clone W6D3), αHLA-DR (clone L243), αIL23p19 (clone 23DCDP). For flow gating we used isotype controls of florescence minus one controls. All the antibodies were purchased from eBioscience or Biolegend
Instrument	BD Fortessa flow cytometer (BD Biosciences).
Software	FlowJo software (10.1)
Cell population abundance	No FACS-sorted done in our experiments
Gating strategy	Data concerning the frequency of different cell subsets analyzed were reported as frequency within the CD45+ cells. CD45+ cells were gated on on FSC-H, FSC-A gate to exclude doublets.

☒ Tick this box to confirm that a figure exemplifying the gating strategy is provided in the Supplementary Information.

Magnetic resonance imaging

Experimental design

Design type	MRI was performed on castrated-Ptenpc-/- mice 0, 4, 8, 12 and 16 weeks after the surgical castration or on CTX IL23wt and CTX IL23ko Ptenpc-/- mice 4, 8, 12 and 16 weeks after the surgical castration.
Design specifications	N/A
Behavioral performance measures	Mice were under general anesthesia by 1.5–2% isoflurane vaporized in 100% oxygen (flow: 1 L/min). Breathing and body temperature were monitored (SA Instruments, Inc., Stony Brook, NY, USA) and maintained around 30 breaths-per-minute and 37°C, respectively.

Acquisition

Imaging type(s)

7T preclinical magnetic resonance scanner (Bruker, BioSpec 70/30 USR, Paravision 5.1), equipped with 450/675 mT/m gradients (slew-rate: 3400–4500T/m/s; rise-time 140 μs) and a mouse body volume coil

Field strength

slew-rate: 3400–4500T/m/s

Sequence & imaging parameters

MRI studies included a Rapid Acquisition with Relaxation Enhancement (RARE) High-Resolution T2-weighted (T2w) sequence with fat suppression acquired in the axial plane (TR =3800ms, TE =45ms, FOV = 27mm x 18mm, spatial resolution = 0,094 x 0,087 mm/pixel, scan time = 8 min, thickness 0.70 mm, 26 slices) and in the coronal plane (TR =3500 ms, TE =38 ms, FOV = 33mm x 33mm, spatial resolution = 0,129 x 0,129 mm/pixel, scan time = 5 min, thickness 0.60 mm, 20 slices).

Area of acquisition

Circumference of the whole prostate was outlined on each RARE T2w axial slice containing identifiable prostate and the number of bounded pixels in each slice was computed and added to yield the prostate volume. Coronal T2w images were used for an accurate identification of the basal and apical limits of the prostate.

Diffusion MRI ☐ Used ☒ Not used

Preprocessing

Preprocessing software

Images were analyzed using NIH software MIPAV (version 7.4.0).

Normalization

NA

Normalization template

NA

Noise and artifact removal

Rarely T2 scan were affected by visible movement artefacts. In this case the scan was immediately repeated after careful control of the depth of the gas anaesthesia and of the correct position of the band used to fix the mouse leg to the bed of the MR scanner. All the stack of T2 weighted images used for the volumetric assessment of prostate volumes were free from visible movement artefacts.

Volume censoring

NA

Statistical modeling & inference

Model type and settings

Waterfall plot depicting proportional change in tumor response was reported.

Effect(s) tested

Statistical analyses (Unpaired Student t test) and One-way ANOVA were used.

Specify type of analysis: ☐ Whole brain ☐ ROI-based ☐ Both

Statistic type for inference
(See Eklund et al. 2016)

NA

Correction

NA

Models & analysis

n/a	Involved in the study
☒ ☐	Functional and/or effective connectivity
☒ ☐	Graph analysis
☒ ☐	Multivariate modeling or predictive analysis